TIME-OF-ARRIVAL ESTIMATION IN OFDM-BASED COGNITIVE RADIO SYSTEMS

A THESIS

SUBMITTED TO THE DEPARTMENT OF ELECTRICAL AND ELECTRONICS ENGINEERING

AND THE INSTITUTE OF ENGINEERING AND SCIENCES

OF BILKENT UNIVERSITY

IN PARTIAL FULFILLMENT OF THE REQUIREMENTS

FOR THE DEGREE OF

MASTER OF SCIENCE

By

Yasir Karışan

July 2010

I certify that I have read this thesis and that in my opinion it is fully adequate, in scope and in quality, as a thesis for the degree of Master of Science.

Assist. Prof. Dr. Sinan Gezici (Supervisor)

I certify that I have read this thesis and that in my opinion it is fully adequate, in scope and in quality, as a thesis for the degree of Master of Science.

Prof. Dr. Orhan Arıkan

I certify that I have read this thesis and that in my opinion it is fully adequate, in scope and in quality, as a thesis for the degree of Master of Science.

Assist. Prof. Dr. İbrahim Körpeoğlu

Approved for the Institute of Engineering and Sciences:

Prof. Dr. Levent Onural
Director of Institute of Engineering and Sciences

ABSTRACT

TIME-OF-ARRIVAL ESTIMATION IN OFDM-BASED COGNITIVE RADIO SYSTEMS

Yasir Karışan
M.S. in Electrical and Electronics Engineering
Supervisor: Assist. Prof. Dr. Sinan Gezici
July 2010

Cognitive radio (CR) systems can efficiently utilize the radio spectrum due to their ability to sense environmental conditions and adapt their communications parameters (such as power, carrier frequency, and modulation) so as to enable dynamic reuse of the available spectrum. In this thesis, theoretical limits on time-of-arrival (TOA) estimation are derived for CR systems in the presence of interference. Specifically, closed form expressions are obtained for Cramer-Rao bounds (CRBs) on TOA estimation in orthogonal frequency division multiplexing (OFDM) based CR systems in various scenarios. Based on the CRB expressions, an optimal power allocation strategy that provides the best possible TOA estimation accuracy is proposed. This strategy considers the constraints imposed by regulatory emission mask and the sensed interference spectrum. The maximum likelihood (ML) TOA estimator is derived for an OFDM-based signalling scheme, and its performance is investigated against the theoretical limits offered by the CRB expressions. In addition, numerical results for the CRBs and ML TOA estimator are obtained and the effects of the optimal power allocation strategy on the accuracy of ML TOA estimator are examined in the absence/presence of interference. The use of optimal power allocation strategy instead of the conventional power assignment scheme is demonstrated to provide significant gains in terms of the TOA estimation accuracy. Analysis of the performance sensitivity of the optimal power allocation strategy to the uncertainty in spectrum estimation is performed, and the performance of optimal power allocation is observed to be consistently superior to that of the uniform power allocation even for substantially high values of spectral estimation errors.

Keywords: Time-of-Arrival (TOA) Estimation, Ranging, Cognitive Radio (CR), Interference, Orthogonal Frequency Divison Multiplexing (OFDM), Cramer-Rao Bound (CRB).

ÖZET

DİKGEN FREKANS BÖLMELİ ÇOĞULLAMAYA DAYALI AKILLI RADYO SİSTEMLERİNDE VARIŞ ZAMANI KESTİRİMİ

Yasir Karışan
Elektrik ve Elektronik Mühendisliği Bölümü Yüksek Lisans
Tez Yöneticisi: Yrd. Doç. Dr. Sinan Gezici
Temmuz 2010

Akıllı radyo sistemleri, çevresel koşulları algılayabilme ve mevcut spektrumun dinamik olarak yeniden kullanımının sağlanması için güç, taşıyıcı frekans, kipleme gibi haberleşme parametrelerini adapte edebilme yetenekleri sayesinde radyo spektrumundan verimli bir şekilde faydalanabilmektedir. Bu tezde, içerisinde girişim barındıran akıllı radyo sistemlerinin varış zamanı (TOA) kestirimi üzerindeki teorik limitler türetilmektedir. Özellikle dikgen frekans bölmeli çoğullamayı (OFDM) temel alan akıllı radyo sistemlerinde çeşitli senaryolar altında varış zamanı kestirimi üzerindeki Cramer-Rao sınırları (CRBs) için kapalı formda ifadeler elde edilmektedir. Cramer-Rao sınırlarını belirten ifadelere dayanılarak, mümkün olan en iyi varış zamanı kestirimi doğruluğu sağlayan en iyi güç atama stratejisi önerilmektedir. Bu strateji düzenleyici yayım maskesi ve algılanan girişim spektrumu tarafından dayatılan kısıtlamaları göz önünde bulundurmaktadır. Dikgen frekans bölmeli çoğullamaya dayalı sinyalizasyon planı için maksimum olabilirlik (ML) kestiricisi türetilmekte, ve bu kestiricinin performansı Cramer-Rao sınırlarını belirten ifadeler tarafından önerilen teorik limitlere karşı incelenmektedir. Ek olarak, Cramer-Rao sınırları ve maksimum olabilirlik varış zamanı kestiricisi için sayısal sonuçlar elde edilmekte ve en iyi güç atama stratejisinin maksimum olabilirlik varış zamanı kestiricisinin doğruluğu üzerindeki etkileri girişim yokluğunda ve varlığında incelenmektedir. Geleneksel eşit dağılımlı güç atama planı yerine, en iyi güç atama stratejisi kullanımının varış zamanı kestiriminin doğruluğu açısından önemli kazançlar sağladığı ispatlanmaktadır. En iyi güç atama stratejisinin performansının spektrum kestirimindeki belirsizliğe karşı olan duyarlılığının analizi gerçekleştirilmekte ve en iyi güç atama stratejisinin performansının geleneksel eşit dağılımlı güç atama planının performansından oldukça yüksek spektrum kestirimi hataları için bile tutarlı bir şekilde daha üstün olduğu gözlenmektedir.

Anahtar Kelimeler: Varış Zamanı Kestirimi, Uzaklık Ölçümü, Akıllı Radyo, Girişim, Dikgen Frekans Bölmeli Çoğullama, Cramer-Rao Sınırı.

ACKNOWLEDGMENTS

I would like to thank my supervisor Assist. Prof. Dr. Sinan Gezici for his invaluable guidance and support throughout my graduate education and thesis research. I do feel myself very lucky that I had an opportunity to work with such an exceedingly understanding and helpful supervisor. I would also like to thank Professors Orhan Arıkan and İbrahim Körpeğlu for being members of my thesis defense committee.

I would also like to thank my family and friends for their endless support and encouragement throughout my graduate study.

Finally, I would like to thank TÜBİTAK BİDEB for its financial support.

Contents

List of Figures

List of Tables

Dedicated to my mother

Chapter 1

Introduction

1.1 Motivation and Related Work

Cognitive radio (CR) is an emerging paradigm that provides efficient and flexible usage of the radio spectrum in the presence of coexisting heterogeneous technologies such as communication and positioning systems [1]-[7]. The main idea behind CR is that a terminal can sense the environment and adapt its features (such as power, carrier frequency, and modulation) so as to enable dynamic reuse of the available spectrum [2]. Recent spectrum measurement campaigns in the United States [8] and Europe [9] indicate that the spectrum resources are under-utilized. Hence, opportunistic use of frequency bands is highly desirable [10].

An important feature of CR systems is location and environment awareness [11]-[18]. A CR device needs to be aware of its location and environment in order to perform adaptation of its system parameters and to facilitate opportunistic spectrum utilization. In addition, the location awareness feature of CRs can be used in system optimization, such as location-assisted spectrum management, handover, routing, dynamic channel allocation and power control [7], [18]. In [11],

[15], and [16], the conceptual models for location and environmental awareness engines and cycles are proposed for CR systems. Also, reference [17] investigates an engine for CR systems via topology information characterization. The cognitive radar concept introduced in [13] can be considered as a mechanism for environmental sensing.

Due to importance of location awareness, a CR device needs to obtain accurate information about its position [11], [12]. A common technique for location determination is based on time-of-arrival (TOA) or range estimation [19]-[22]. CR devices can estimate their locations based on TOA measurements of signals traveling between them.

Since a CR system operates in an environment where the spectrum is utilized in a dynamic manner, the range/TOA estimation problem becomes more challenging than that in conventional systems. In [23], the theoretical limits on range estimation are studied for dispersed spectrum CR systems. A receiver with multiple branches is considered, where each branch processes a narrowband signal at a different center frequency. The Cramer-Rao bounds (CRBs) on range estimation are obtained. In [10] the same problem is considered and practical two-step range estimation algorithms are proposed. It is observed that the frequency diversity in the system can be utilized for range estimation.

Unlike references [10] and [23], where a number of narrowband signals at different center frequencies are considered, the waveform transmitted by a CR system can also be modeled as a single orthogonal frequency division multiplexing (OFDM) signal [24]-[26]. Correspondingly, the coefficients of the subcarriers can be adjusted in various ways so as to provide spectrum agility, capacity improvement, or range accuracy enhancement [27].

The present thesis assumes OFDM signalling and investigates the theoretical limits on CR range estimation. As CR devices need to operate in the presence of interference, the effects of interference are also considered. Thus, our study [28] derives CRB expressions for range estimation in the presence of interference. Although [29] deals with a related issue and focuses on the problem of sampling clock frequency mismatch between a transmitter and a receiver in an OFDM system, the CRB expressions obtained in that study are concerned with the estimation of clock frequency offset between the transmitter and the receiver, and it is assumed that no interference exists in the system. In addition, in our study, an optimal power allocation strategy is proposed for minimizing the CRB on time delay estimation under practical constraints (such as the regulatory limits on the transmission power spectral density), and a maximum likelihood (ML) TOA estimation algorithm is investigated in order to assess the effects of the optimal power allocation algorithm in practical systems. Numerical results and simulation examples are provided to compare conventional and optimal power allocation strategies. Channel delay estimation is also addressed in [30] in the context of multiple-input multiple-output OFDM systems. The resulting algorithms, however, are more complex than those discussed in the present thesis because the main concern in [30] is to separate signals arriving from different transmitting antennas.

In principle, the problem studied in this thesis can be regarded as a pure estimation problem. However, the CR framework seems to be more appropriate due to the following reasons. First, it is assumed that knowledge of the interference spectrum has to be acquired by the system, which implies the presence of a *spectrum sensing* unit that is typical of CR systems [4], [11]. Also, feedback from receiver to transmitter is needed in practice to allow the transmitter to learn the channel characteristics and adapt its parameters accordingly, which is again a common feature of CR systems [7]. In short, sensing, awareness, learning, and adaptation features of CR systems are assumed in this thesis [4], [11].

1.2 Contributions of the Thesis

The main contributions of this thesis can be summarized as follows:

- A closed-form expression of the CRB is obtained for range estimation in OFDM-based CR systems in the presence of interference.
- An optimal power allocation (or, spectrum shaping) strategy that offers the best possible TOA estimation accuracy is proposed based on CRB expressions.
- The ML TOA estimator is derived for OFDM-based signalling scheme and its performance is investigated against the theoretical limits
- The use of optimal optimal power allocation strategy instead of the conventional uniform power assignment scheme is demonstrated to bring in significant gains in terms of TOA estimation accuracy in some practical scenarios.
- Analysis of the performance sensitivity of the optimal power allocation strategy to the uncertainty in spectrum estimation is performed, and the performance of optimal power allocation is shown to be consistently superior to that of the uniform allocation even for substantially high values of spectral estimation errors.

1.3 Thesis Organization

The remainder of the thesis is organized as follows. In Chapter 2, an OFDM-based signal model is introduced for CR systems. Various CRBs for TOA estimation are derived in the presence of interference due, for example, to the existence of one or more communication systems sharing the same spectrum.

The CRB expressions are then exploited to formulate the optimal power allocation scheme (i.e., the transmitted signal spectrum shape) that maximizes the range estimation accuracy under constraints coming both from the regulatory transmitted signal spectrum mask and the sensed interference spectrum.

In Chapter 3, the ML TOA estimator is derived for OFDM-based signalling scheme introduced in Chapter 2, and its performance is analyzed against the theoretical limits offered by the CRB expressions presented in Chapter 2. Numerical results for the CRBs are obtained and the effects of the optimal weight selection on the accuracy of ML TOA estimator are investigated in the absence/presence of interference. Also, analysis results for the performance sensitivity of the optimal power allocation scheme to the spectrum estimation errors are presented.

In Chapter 4, the thesis is brought to a conclusion with a brief overview of the research findings presented so far, and the possible future research topics are discussed.

Chapter 2

CRBs on Time-of-Arrival Estimation in OFDM-Based CR Systems

This chapter is organized as follows. In Section 2.1, an OFDM-based signal model is introduced for CR systems. In Section 2.2, various CRBs for TOA estimation are derived for the OFDM-based signalling scheme in the presence of interference. Finally, in Section 2.3 , the CRB expressions are exploited to formulate the optimal power allocation strategy that maximizes the TOA estimation accuracy under the constraints imposed by the regulatory transmitted signal spectrum mask and the sensed interference spectrum.

2.1 Signal Model

Thanks to their flexibility in utilizing the radio spectrum, multicarrier signals are commonly employed in CR systems [24]. In this thesis, a signalling scheme of this type is adopted and the transmitted baseband signal is modeled as

$$s(t) = \sum_{k=1}^{K} \sqrt{w_k}\, p(t)\, e^{\jmath 2\pi f_k t} \,, \tag{2.1}$$

over the symbol interval $[-T_s/2, T_s/2]$. In this equation, $f_k = (k - K/2)\Delta$ is the kth subcarrier frequency shift with respect to the center frequency, Δ is the subcarrier spacing, and $p(t)$ is a pulse with duration T_s and energy E_p. A guard interval between symbols is assumed to be inserted to avoid inter-symbol interference at the receiver. The weights $w_k \geq 0$ enable spectrum shaping and

$$P_t = \frac{E_p}{T_s} \sum_{k=1}^{K} w_k \tag{2.2}$$

represents the power of the baseband signal. The corresponding passband RF power is $\frac{E_p}{2T_s} \sum_{k=1}^{K} w_k$. In practice, the weights w_k are limited by peak power constraints, as it is detailed in Section 2.3 when investigating the optimal signal spectrum minimizing the CRBs on range estimation.

Assuming that Δ is small compared to the channel coherence bandwidth, the baseband received signal corresponding to (2.1) is

$$r(t) \cong s_r(t - \tau) + z(t) \,, \tag{2.3}$$

with

$$s_r(t) = \sum_{k=1}^{K} \alpha_k \sqrt{w_k}\, p(t)\, e^{\jmath 2\pi f_k t} \,, \tag{2.4}$$

where τ is the propagation delay, $\alpha_k = a_k e^{\jmath \phi_k}$ denotes the complex channel coefficient at frequency f_k and $z(t)$ is the total disturbance due to thermal noise and interference. In particular, $z(t)$ is the sum of two terms, say $z_N(t)$ and $z_I(t)$, where $z_N(t)$ is complex additive white Gaussian noise (AWGN) with spectral density N_0 for each component, and $z_I(t)$ is a stationary interference term with power spectral density $S_I(f)$ for each component. Thus, the power spectral density of each component of $z(t)$ is $S_z(f) = N_0 + S_I(f)$. The interference is modeled as a zero-mean complex Gaussian process. Considering a CR framework, it is assumed that $S_I(f)$ is known at the receiver [1]-[3].

It should be noted that the received signal model in (2.3)-(2.4) applies to a multipath channel, and the propagation delay τ represents the delay of the shortest path. For example, with line-of-sight propagation, τ coincides with the delay of the direct path, and under such conditions, τ is related to the range (distance) between the transmitter and the receiver. Based on a number of range estimates, between a device and a number of reference devices, the position of a device can be estimated [20].

2.2 CRBs on TOA Estimation in the Presence of Interference

In this section we consider the best achievable accuracy in estimating the TOA parameter τ from the observation of $r(t)$. The observation interval is assumed to be sufficiently long so as to comprise the whole received signal notwithstanding the *a priori* uncertainty on the actual value of τ. It is further assumed that information on the interference spectral density $S_I(f)$ is available from the spectrum awareness engine of CR [11], [12]. The Fourier transform $\mathscr{F}\{s_r(t-\tau)\}$ of $s_r(t-\tau)$ in (2.4) is

$$S_r(f,\boldsymbol{\theta}) = \int_{-\infty}^{\infty} s_r(t-\tau)\, e^{-\jmath 2\pi f t}\, \mathrm{d}t = \sum_{k=1}^{K} \alpha_k \sqrt{w_k}\, P(f-f_k)\, e^{-\jmath 2\pi f \tau} \;, \qquad (2.5)$$

where $P(f)$ is the Fourier transform of $p(t)$, and $\boldsymbol{\theta} \triangleq [\tau \; a_1 \cdots a_K \; \phi_1 \cdots \phi_K]$ is a vector collecting all the channel parameters. In computing the CRB for the estimation of τ, two different approaches can be adopted. In one case, called *joint bounding*, the estimation process concerns all the components of $\boldsymbol{\theta}$ and a bound is derived for each of them. In the other case, the focus is on τ alone and the other components of $\boldsymbol{\theta}$ are regarded as known parameters. This is referred to as *conditional bounding* [32].

2.2.1 Joint Bounding

As the disturbance $z(t)$ is colored, we assume without loss of generality that the received signal is first passed though a whitening filter with a frequency response [33]

$$|H(f)|^2 = \frac{1}{S_z(f)} \; . \tag{2.6}$$

Accordingly, the log-likelihood function can be written as [1]

$$\ln \Lambda(\widetilde{\boldsymbol{\theta}}) = \Re \left\{ \int\limits_{-\infty}^{\infty} x(t) u^*(t, \widetilde{\boldsymbol{\theta}}) \mathrm{d}t \right\} - \frac{1}{2} \int\limits_{-\infty}^{\infty} \left| u(t, \widetilde{\boldsymbol{\theta}}) \right|^2 \mathrm{d}t \tag{2.7}$$

where $\widetilde{\boldsymbol{\theta}}$ is a possible value of $\boldsymbol{\theta}$, $x(t) = r(t) \otimes h(t)$ is the convolution of the received waveform $r(t)$ with the impulse response of the whitening filter $h(t)$, $u(t, \widetilde{\boldsymbol{\theta}}) = \tilde{s}_r(t - \tilde{\tau}) \otimes h(t)$, and

$$\tilde{s}_r(t) = \sum_{k=1}^{K} \tilde{\alpha}_k \sqrt{w_k}\, p(t)\, e^{\jmath 2\pi f_k t}. \tag{2.8}$$

Derivation of (2.7) be found in Appendix A.1.

Equivalently, the whitening operation can be performed by correlating $r(t)$ with a pulse $g(t, \widetilde{\boldsymbol{\theta}})$ with the following Fourier transform [33]

$$G(f, \widetilde{\boldsymbol{\theta}}) \propto \tilde{S}_r(f, \widetilde{\boldsymbol{\theta}}) / S_z(f) \tag{2.9}$$

where $\tilde{S}_r(f, \widetilde{\boldsymbol{\theta}}) = \mathscr{F}\left\{\tilde{s}_r(t - \tilde{\tau})\right\}$ and the log-likelihood function is obtained as [33]

$$\ln \Lambda(\widetilde{\boldsymbol{\theta}}) = \Re \left\{ \int\limits_{-\infty}^{\infty} r(t)\, g^*(t, \widetilde{\boldsymbol{\theta}}) \mathrm{d}t \right\} - \frac{1}{2} \int\limits_{-\infty}^{\infty} \tilde{s}_r(t - \tilde{\tau})\, g^*(t, \widetilde{\boldsymbol{\theta}}) \mathrm{d}t. \tag{2.10}$$

Derivation of (2.9) and (2.10) can be found in Appendix A.2.

The CRB for TOA estimation is computed as

$$\mathrm{Var}\left(\hat{\tau}\right) \geq \left[\mathbf{J}^{-1}\right]_{1,1} = \mathrm{CRB} \; , \tag{2.11}$$

[1] $\Re\{x\}$ and $\Im\{x\}$ denote the real and the imaginary parts of x, respectively.

where $\mathbf{J}$ is the Fisher information matrix (FIM) with elements [33]

$$[\mathbf{J}]_{m,n} = \Re\left\{\int_{-\infty}^{\infty} \frac{\partial \tilde{S}_r^*(f,\boldsymbol{\theta})}{\partial \tilde{\theta}_m}\, S_z^{-1}(f)\, \frac{\partial \tilde{S}_r(f,\boldsymbol{\theta})}{\partial \tilde{\theta}_n} \mathrm{d}f \right\}. \tag{2.12}$$

In (2.12), $\tilde{\theta}_n$ is the nth element of $\widetilde{\boldsymbol{\theta}}$, and with a slight abuse of notation, $\partial \tilde{S}_r(f,\boldsymbol{\theta})/\partial \tilde{\theta}_n$ denotes the partial derivative of $\tilde{S}_r(f,\boldsymbol{\theta})$ with respect to $\tilde{\theta}_n$ computed for $\boldsymbol{\theta} = \widetilde{\boldsymbol{\theta}}$.

After some manipulations from (2.5) and (2.12) it is found that [2]

$$\mathbf{J} = \begin{bmatrix} \mathrm{J}_{\tau\tau} & \mathbf{J}_{\tau a} & \mathbf{J}_{\tau\phi} \\ \mathbf{J}_{\tau a}^T & \mathbf{J}_{aa} & \mathbf{J}_{a\phi} \\ \mathbf{J}_{\tau\phi}^T & \mathbf{J}_{a\phi}^T & \mathbf{J}_{\phi\phi} \end{bmatrix} \tag{2.13}$$

where the elements of $\mathbf{J}$ are as expressed in Appendix A.3.

Inspection of (2.13) reveals that the FIM can be put into the form of

$$\mathbf{J} = \begin{bmatrix} \mathrm{J}_{\tau\tau} & \mathbf{B} \\ \mathbf{B}^T & \mathbf{C} \end{bmatrix}, \tag{2.14}$$

with

$$\mathbf{B} \triangleq \begin{bmatrix} \mathbf{J}_{\tau a} & \mathbf{J}_{\tau\phi} \end{bmatrix}, \tag{2.15}$$

and

$$\mathbf{C} \triangleq \begin{bmatrix} \mathbf{J}_{aa} & \mathbf{J}_{a\phi} \\ \mathbf{J}_{a\phi}^T & \mathbf{J}_{\phi\phi} \end{bmatrix}. \tag{2.16}$$

Thus, substituting (2.14) into (2.11), and assuming invertibility of $\mathbf{C}$ yields

$$\mathrm{CRB} = \left(\mathrm{J}_{\tau\tau} - \mathbf{B}\mathbf{C}^{-1}\mathbf{B}^{\mathrm{T}}\right)^{-1} \tag{2.17}$$

Equation (2.17) takes simpler forms in the following special cases. So far in the discussion, $\tilde{a}_k$, $\tilde{\phi}_k$, and $\tilde{\tau}$ have been used to represent possible values of the channel parameters a_k, ϕ_k, and τ. From now on, they will be replaced by a_k, ϕ_k, and τ for the sake of notational simplicity.

[2] $\mathbf{A}^{\mathbf{T}}$ is the transpose of $\mathbf{A}$.

2.2.1.1 Disjoint Spectra

If $|P(f)|$ is approximately zero outside $-\Delta/2 \leq f \leq \Delta/2$, from (A.17) we have $y_{m,n}(i) = 0$ for $m \neq n$ and (A.18)–(A.23) become

$$\mathrm{J}_{\tau\tau} = 4\pi^2 \sum_{k=1}^{K} |\alpha_k|^2 \; w_k \, \eta_k(2) \; , \tag{2.18}$$

$$\mathbf{J}_{\tau a} = \mathbf{0} \; , \tag{2.19}$$

$$[\mathbf{J}_{\tau\phi}]_m = -2\pi \, w_m \, |\alpha_m|^2 \, \eta_m(1) \; , \tag{2.20}$$

$$\mathbf{J}_{aa} = \mathrm{diag}\left\{w_1 \, \eta_1(0), w_2 \, \eta_2(0), \ldots, w_K \, \eta_K(0)\right\} \; , \tag{2.21}$$

$$\mathbf{J}_{a\phi} = \mathbf{0} \; , \tag{2.22}$$

$$\mathbf{J}_{\phi\phi} = \mathrm{diag}\left\{w_1 \; |\alpha_1|^2 \; \eta_1(0), w_2 \; |\alpha_2|^2 \; \eta_2(0), \ldots, w_K \; |\alpha_K|^2 \; \eta_K(0)\right\} \; , \tag{2.23}$$

with

$$\eta_k(i) \triangleq \int_{-\infty}^{\infty} f^i S_z^{-1}(f) \, |P(f - f_k)|^2 \, \mathrm{d}f \; , \quad i = 0, 1, 2 \; . \tag{2.24}$$

Thus, substituting (2.18)–(2.23) into (2.17) yields

$$\mathrm{CRB} = \left(\mathrm{J}_{\tau\tau} - \mathbf{J}_{\tau\phi}\mathbf{J}_{\phi\phi}^{-1}\mathbf{J}_{\tau\phi}^{\mathrm{T}}\right)^{-1} = \left(\sum_{k=1}^{K} w_k \, \lambda_k\right)^{-1} \; , \tag{2.25}$$

with

$$\lambda_k \triangleq 4\pi^2 \, |\alpha_k|^2 \left(\eta_k(2) - \frac{\eta_k^2(1)}{\eta_k(0)}\right) \; . \tag{2.26}$$

We see that the contribution of each subcarrier to the CRB is determined by the corresponding weight w_k, the squared channel gain $|\alpha_k|^2$, the spectrum of pulse $p(t)$, and the power spectral density $S_I(f)$ of the interference around f_k. Derivation of (2.25) can be found in Appendix A.4.

2.2.1.2 Slowly Varying $\mathbf{S_z(f)}$

The coefficient λ_k in (2.26) can be further simplified assuming $S_z(f) \cong S_z(f_k) = N_0 + S_I(f_k)$ for $|f - f_k| \leq \Delta/2 \ \forall k$. Correspondingly (2.24) becomes

$$\begin{aligned}\eta_k(i) &\cong \frac{1}{S_z(f_k)} \int\limits_{-\infty}^{\infty} f^i \left|P(f - f_k)\right|^2 \mathrm{d}f \\ &= \frac{1}{S_z(f_k)} \int\limits_{-\infty}^{\infty} (f + f_k)^i \left|P(f)\right|^2 \mathrm{d}f.\end{aligned} \tag{2.27}$$

Then, defining

$$\beta_i \triangleq \frac{1}{E_p} \int\limits_{-\infty}^{\infty} f^i \left|P(f)\right|^2 \mathrm{d}f \qquad i = 0, 1, 2 \tag{2.28}$$

and bearing in mind that

$$\int\limits_{-\infty}^{\infty} \left|P(f)\right|^2 \mathrm{d}f = E_p, \tag{2.29}$$

we obtain

$$\lambda_k = \frac{4\pi^2 E_p \left|\alpha_k\right|^2 \left(\beta_2 - \beta_1^2\right)}{N_0 + S_I(f_k)} \ , \tag{2.30}$$

which results from the substitution of (2.27)–(2.29) into (2.26). Derivation of (2.30) can be found in Appendix A.5.

The physical meanings of β_2 and β_1 are as follows: From (2.28) we recognize that the former gives the *mean-squared bandwidth* of $p(t)$ while the latter represents the *skewness* of the spectrum $|P(f)|^2$. Note that if $p(t)$ is real valued $|P(f)|$ is an even function and β_1 is zero.

Equation (2.30) indicates that the contribution of the kth subcarrier is proportional to $\left|\alpha_k\right|^2/(N_0 + S_I(f_k))$. Thus, λ_k gets larger and the CRB reduces as the channel gain increases and/or the interference spectral density around f_k decreases.

2.2.2 Conditional Bounding

Assuming that the components of $\boldsymbol{\theta}$ are all known except for τ, the CRB for TOA estimation can be derived from (2.11)–(2.12) by considering the estimation of a single parameter. As a result we get

$$\text{CRB} = \int_{-\infty}^{\infty} \frac{1}{S_z(f)} \left| \frac{\partial \tilde{S}_r(f, \boldsymbol{\theta})}{\partial \tilde{\theta}_n} \right|^2 \mathrm{d}f = [\mathrm{J}_{\tau\tau}]^{-1} \ , \tag{2.31}$$

where $\mathrm{J}_{\tau\tau}$ is still as in (A.18). Comparison with (2.25) reveals that the conditional bound is equal to or less than the joint bound. This is intuitively clear because precise information on parameters $[a_1 \cdots a_K \ \phi_1 \cdots \phi_K]$ is assumed to be available in (2.31).

2.2.2.1 Disjoint Spectra and Slowly Varying $\mathbf{S_z(f)}$

In this case, $\mathrm{J}_{\tau\tau}$ and $\eta_k(2)$ are given by (2.18) and (A.36), respectively. Thus, the CRB takes the same form as in the joint bounding case (cf. (2.25)):

$$\text{CRB} = [\mathrm{J}_{\tau\tau}]^{-1} = \left(\sum_{k=1}^{K} w_k \, \bar{\lambda}_k \right)^{-1} \ , \tag{2.32}$$

with

$$\bar{\lambda}_k \triangleq \frac{4\pi^2 E_p \left|\alpha_k\right|^2 (\beta_2 + 2 f_k \beta_1 + f_k^2)}{N_0 + S_I(f_k)} \ . \tag{2.33}$$

Note that the difference

$$\begin{aligned} \bar{\lambda}_k - \lambda_k &= \frac{4\pi^2 E_p \left|\alpha_k\right|^2 (\beta_2 + 2 f_k \beta_1 + f_k^2)}{N_0 + S_I(f_k)} - \frac{4\pi^2 E_p \left|\alpha_k\right|^2 (\beta_2 - \beta_1^2)}{N_0 + S_I(f_k)} \\ &= \frac{4\pi^2 E_p \left|\alpha_k\right|^2 (\beta_1 + f_k)^2}{N_0 + S_I(f_k)} \end{aligned} \tag{2.34}$$

is non-negative so that $\bar{\lambda}_k \geq \lambda_k$. This agrees with our intuition that conditional bounding gives a lower CRB than joint bounding.

2.3 Optimal Weights

Now we concentrate on the weight assignment that minimizes the CRB. The optimal weights must satisfy constraints on the emitted signal spectrum imposed by regulatory masks (for example, the FCC mask for ultra-wide bandwidth signals [36]). Let $B(f)$ denote the equivalent baseband version of the power spectral density mask. Then, defining $\boldsymbol{w} \triangleq (w_1, w_2, \cdots, w_k)^T$ and $\boldsymbol{\lambda} \triangleq (\lambda_1, \lambda_2, \cdots, \lambda_K)$ (cf. (2.25) and (2.32)), the optimal weights are found as the solution of the following optimization problem:

$$\underset{\boldsymbol{w}}{\text{maximize}} \quad \boldsymbol{\lambda}^T \boldsymbol{w} \tag{2.35}$$

subject to

$$\mathbf{1}^T \boldsymbol{w} \leq 1 \tag{2.36}$$

$$\boldsymbol{w} \succeq \mathbf{0} \tag{2.37}$$

$$\boldsymbol{w} \preceq \boldsymbol{b} \tag{2.38}$$

where $\boldsymbol{x} \preceq \boldsymbol{y}$ means that each element of $\boldsymbol{x}$ is smaller than or equal to the corresponding element of $\boldsymbol{y}$, $\mathbf{1}$ is the vector of all ones, $\boldsymbol{b} \triangleq [b_1 \; b_2 \cdots b_K]^T$, and $b_k \triangleq B(f_k)\Delta/P_t$ is the normalized emission power constraint on the kth subcarrier.

This is a classical linear programming problem and its solution is obtained in closed-form as indicated in the following proposition.

Proposition 1: *Without loss of generality, assume that the λ_k's are in a decreasing order* [3], *i.e., $\lambda_1 > \lambda_2 > \cdots > \lambda_K$. Then, the optimal weights are recursively computed as*

$$w_i^{(\text{opt})} = \min \left\{ b_i \, , 1 - \sum_{j=1}^{i-1} w_j^{(\text{opt})} \right\} \; , \tag{2.39}$$

[3] The solution can easily be extended to the case in which two or more λ_k's are equal.

for $i = 2, 3, \ldots, K,$ *with* $w_1^{(\mathrm{opt})} = \min\{1, b_1\}$.

Proof: See Appendix A.6.

An alternative way of writing (2.39) is

$$\begin{aligned} w_1^{(\mathrm{opt})} &= \min\{1, b_1\} \ , \\ w_2^{(\mathrm{opt})} &= \min\left\{1 - w_1^{(\mathrm{opt})}, b_2\right\} \ , \\ w_3^{(\mathrm{opt})} &= \min\left\{1 - w_1^{(\mathrm{opt})} - w_2^{(\mathrm{opt})}, b_3\right\} \ , \\ &\vdots \end{aligned} \tag{2.40}$$

and so on. This result has the following intuitive interpretation. We start with selecting the *best* subcarrier (the one associated with the largest component of $\boldsymbol{\lambda}$) and we assign to it the maximum allowed power, which is $\min\{1, b_1\}$. Next, we select the best of the remaining subcarriers (the one associated with the second largest component of $\boldsymbol{\lambda}$) and again assign to it the maximum allowed power (which is the minimum between b_2 and the residual power $1 - w_1^{(\mathrm{opt})}$). We proceed in this way until all the available power is used or no other subcarriers are available (which happens if $\sum_{i=1}^{K} b_i \leq 1$).

Chapter 3

Performance Evaluation and Numerical Examples

This chapter is organized as follows. In Section 3.1, the ML TOA estimator is derived for the OFDM-based signal model elaborated in Chapter 2. In Section 3.2, numerical evaluations of the CRBs are presented. The performance of the ML TOA estimator is analyzed against the theoretical limits offered by the CRB expressions presented in Chapter 2, and the effects of the optimal weight selection on the accuracy of ML TOA estimator are investigated in the absence/presence of interference. Finally, analysis results for the performance sensitivity of the optimal power allocation scheme to the uncertainty in spectrum estimation are presented in Section 3.2.

3.1 ML TOA Estimation Algorithm

In order to derive the ML TOA estimator [39], we start from the log-likelihood function in (2.7). Defining

$$g_k(t) \triangleq \sqrt{w_k}\, p(t)\, e^{\jmath 2\pi f_k t} \otimes h(t) \tag{3.1}$$

$$x_k\left(\tilde{\tau}\right) \triangleq \int_{-\infty}^{\infty} x(t) g_k^*(t-\tilde{\tau})\mathrm{d}t \tag{3.2}$$

$$\rho_{k,l} \triangleq \int_{-\infty}^{\infty} g_k^*(t-\tilde{\tau}) g_l(t-\tilde{\tau})\mathrm{d}t \tag{3.3}$$

and taking (2.8) into account yields

$$\begin{aligned}
\ln\Lambda(\widetilde{\boldsymbol{\theta}}) &= \Re\left\{\int_{-\infty}^{\infty} x(t) u^*(t,\widetilde{\boldsymbol{\theta}})\mathrm{d}t\right\} - \frac{1}{2}\int_{-\infty}^{\infty}\left|u(t,\widetilde{\boldsymbol{\theta}})\right|^2 \mathrm{d}t \\
&= \Re\left\{\int_{-\infty}^{\infty} x(t)\left[\tilde{s}_r(t-\tilde{\tau})\otimes h(t)\right]^* \mathrm{d}t\right\} - \frac{1}{2}\int_{-\infty}^{\infty}\left|\tilde{s}_r(t-\tilde{\tau})\otimes h(t)\right|^2 \mathrm{d}t \\
&= \Re\left\{\int_{-\infty}^{\infty} x(t)\left[\sum_{k=1}^{K}\tilde{\alpha}_k\sqrt{w_k}\, p(t-\tilde{\tau}) e^{\jmath 2\pi f_k (t-\tilde{\tau})}\otimes h(t)\right]^* \mathrm{d}t\right\} - \\
&\quad \frac{1}{2}\int_{-\infty}^{\infty}\left|\sum_{k=1}^{K}\tilde{\alpha}_k\sqrt{w_k}\, p(t-\tilde{\tau}) e^{\jmath 2\pi f_k (t-\tilde{\tau})}\otimes h(t)\right|^2 \mathrm{d}t \\
&= \Re\left\{\int_{-\infty}^{\infty} x(t)\left[\sum_{k=1}^{K}\tilde{\alpha}_k g_k(t-\tilde{\tau})\right]^* \mathrm{d}t\right\} - \frac{1}{2}\int_{-\infty}^{\infty}\left|\sum_{k=1}^{K}\tilde{\alpha}_k g_k(t-\tilde{\tau})\right|^2 \mathrm{d}t \\
&= \Re\left\{\sum_{k=1}^{K}\tilde{\alpha}_k^* \int_{-\infty}^{\infty} x(t) g_k^*(t-\tilde{\tau})\mathrm{d}t\right\} - \\
&\quad \frac{1}{2}\sum_{k=1}^{K}\sum_{l=1}^{K}\tilde{\alpha}_k^*\tilde{\alpha}_l \int_{-\infty}^{\infty} g_k^*(t-\tilde{\tau}) g_l(t-\tilde{\tau})\mathrm{d}t \\
&= \Re\left\{\sum_{k=1}^{K}\tilde{\alpha}_k^* x_k(\tilde{\tau})\right\} - \frac{1}{2}\sum_{k=1}^{K}\sum_{l=1}^{K}\tilde{\alpha}_k^*\tilde{\alpha}_l\rho_{k,l}.
\end{aligned} \tag{3.4}$$

Using a matrix notation, (3.4) can be written as

$$\begin{aligned}\ln\Lambda(\widetilde{\boldsymbol{\theta}}) &= \Re\left\{\widetilde{\boldsymbol{\alpha}}^H\mathbf{x}(\tilde{\tau})\right\} - \frac{1}{2}\widetilde{\boldsymbol{\alpha}}^H\mathbf{R}\widetilde{\boldsymbol{\alpha}} \\ &= \frac{1}{2}\left(\widetilde{\boldsymbol{\alpha}}^H\mathbf{x}(\tilde{\tau}) + \mathbf{x}^H(\tilde{\tau})\widetilde{\boldsymbol{\alpha}} - \widetilde{\boldsymbol{\alpha}}^H\mathbf{R}\widetilde{\boldsymbol{\alpha}}\right)\end{aligned} \tag{3.5}$$

where $\widetilde{\boldsymbol{\alpha}} \triangleq [\tilde{\alpha}_1, \tilde{\alpha}_2, \ldots, \tilde{\alpha}_K]^T$, $\mathbf{x}(\tilde{\tau}) \triangleq [x_1(\tilde{\tau}), x_2(\tilde{\tau}), \ldots, x_K(\tilde{\tau})]^T$, and $\mathbf{R}$ is the $K \times K$ Hermitian symmetric correlation matrix

$$\mathbf{R} \triangleq \begin{bmatrix} \rho_{1,1} & \rho_{1,2} & \cdots & \rho_{1,K} \\ \rho_{2,1} & \rho_{2,2} & \cdots & \rho_{2,K} \\ \vdots & \vdots & \ddots & \vdots \\ \rho_{K,1} & \rho_{K,2} & \cdots & \rho_{K,K} \end{bmatrix}. \tag{3.6}$$

Our goal is to maximize (3.5) with respect to $\tilde{\tau}$ and $\widetilde{\boldsymbol{\alpha}}$. To this purpose, $\tilde{\tau}$ is initially taken as fixed and $\widetilde{\boldsymbol{\alpha}}$ is allowed to vary. The $\widehat{\boldsymbol{\alpha}}$ that maximizes (3.5) is computed by taking the derivative of (3.5) with respect to $\widetilde{\boldsymbol{\alpha}}$, and equating the result to zero.

$$\frac{\partial \ln\Lambda(\widetilde{\boldsymbol{\theta}})}{\partial\widetilde{\boldsymbol{\alpha}}} = \frac{1}{2}\left(\mathbf{x}^*(\tilde{\tau}) - \mathbf{R}^T\widetilde{\boldsymbol{\alpha}}^*\right) = \mathbf{0} \tag{3.7}$$

Then, $\widehat{\boldsymbol{\alpha}}$ is found to be

$$\widehat{\boldsymbol{\alpha}} = \mathbf{R}^\dagger\mathbf{x}(\tilde{\tau}), \tag{3.8}$$

where $\mathbf{R}^\dagger$ stands for the pseudo-inverse of $\mathbf{R}$. Next, substituting (3.8) into (3.5) and maximizing with respect to $\tilde{\tau}$ produces

$$\begin{aligned}\hat{\tau} &= \arg\max_{\tilde{\tau}} \left\{\Re\left\{\widehat{\boldsymbol{\alpha}}^H\mathbf{x}(\tilde{\tau})\right\} - \frac{1}{2}\widehat{\boldsymbol{\alpha}}^H\mathbf{R}\widehat{\boldsymbol{\alpha}}\right\} \\ &= \arg\max_{\tilde{\tau}} \left\{\frac{1}{2}\left(\widehat{\boldsymbol{\alpha}}^H\mathbf{x}(\tilde{\tau}) + \mathbf{x}^H(\tilde{\tau})\widehat{\boldsymbol{\alpha}} - \widehat{\boldsymbol{\alpha}}^H\mathbf{R}\widehat{\boldsymbol{\alpha}}\right)\right\} \\ &= \arg\max_{\tilde{\tau}} \left\{\mathbf{x}(\tilde{\tau})^H\mathbf{R}^\dagger\mathbf{x}(\tilde{\tau}) + \mathbf{x}(\tilde{\tau})^H\mathbf{R}^\dagger\mathbf{x}(\tilde{\tau}) - \mathbf{x}(\tilde{\tau})^H\mathbf{R}^\dagger\mathbf{R}\mathbf{R}^\dagger\mathbf{x}(\tilde{\tau})\right\} \\ &= \arg\max_{\tilde{\tau}} \left\{\mathbf{x}(\tilde{\tau})^H\mathbf{R}^\dagger\mathbf{x}(\tilde{\tau})\right\}\end{aligned} \tag{3.9}$$

where the passage from the third to the fourth line follows from the pseudo-inverse property that $\mathbf{R}^\dagger\mathbf{R}\mathbf{R}^\dagger = \mathbf{R}^\dagger$.

The last expression in (3.9) gives the desired ML estimate of τ. The ML estimate of $\boldsymbol{\alpha}$ is obtained from (3.8) by replacing $\tilde{\tau}$ with $\hat{\tau}$ as follows

$$\widehat{\boldsymbol{\alpha}} = \mathbf{R}^{\dagger}\mathbf{x}\left(\arg\max_{\widetilde{\tau}} \quad \left\{\mathbf{x}(\tilde{\tau})^{H}\mathbf{R}^{\dagger}\mathbf{x}(\tilde{\tau})\right\}\right). \tag{3.10}$$

Equation (3.9) can be further simplified in the following special cases.

3.1.1 Disjoint Spectra

If $|P(f)|$ is approximately zero outside $-\Delta/2 \leq f \leq \Delta/2$, from (3.3) we have

$$\begin{aligned} \rho_{k,l} &= \int_{-\infty}^{\infty} g_k^*(t-\tilde{\tau})g_l(t-\tilde{\tau})\mathrm{d}t \\ &= \int_{-\infty}^{\infty} g_k^*(t)g_l(t)\mathrm{d}t \\ &= \int_{-\infty}^{\infty} G_k^*(f)G_l(f)\mathrm{d}f \\ &= \sqrt{w_k}\sqrt{w_l}\int_{-\infty}^{\infty} P^*(f-f_k)P(f-f_l)\left|H(f)\right|^2\mathrm{d}f \\ &= \delta_{k\,l}\left\{w_k\int_{-\infty}^{\infty}\left|P(f-f_k)\right|^2\left|H(f)\right|^2\mathrm{d}f\right\}, \end{aligned} \tag{3.11}$$

where the passage from the second to the third line follows from Parseval's theorem, $g_k(t)$ is as defined in (3.1), and $\delta_{k\,l}$ is the Kronecker delta function defined as

$$\delta_{k\,l} = \begin{cases} 1 \;, & \text{if} \quad k = l \\ 0 \;, & \text{if} \quad k \neq l \end{cases}. \tag{3.12}$$

Then, the correlation matrix $\mathbf{R}$ in (3.6) becomes

$$\mathbf{R} = \begin{bmatrix} \rho_{1,1} & 0 & \cdots & 0 \\ 0 & \rho_{2,2} & \cdots & 0 \\ \vdots & \vdots & \ddots & \vdots \\ 0 & 0 & \cdots & \rho_{K,K} \end{bmatrix} \tag{3.13}$$

with

$$\rho_{k,k} = w_k \int\limits_{-\infty}^{\infty} |P(f - f_k)|^2 \, |H(f)|^2 \, \mathrm{d}f. \tag{3.14}$$

Substituting $\mathbf{R}$ in (3.13) into $\hat{\tau}$ in (3.9), we get

$$\begin{aligned} \hat{\tau} &= \arg \max_{\tilde{\tau}} \quad \left\{ \mathbf{x}(\tilde{\tau})^H \mathbf{R}^{\dagger} \mathbf{x}(\tilde{\tau}) \right\} \\ &= \arg \max_{\tilde{\tau}} \quad \left\{ \sum_{\substack{k=1 \\ \rho_{k,k} \neq 0}}^{K} \rho_{k,k}^{-1} \left| x_k \left(\tilde{\tau} \right) \right|^2 \right\}. \end{aligned} \tag{3.15}$$

It should be noted that ML TOA estimator in (3.15) requires a simple one-dimensional search which results in a low-complexity solution. The exact computational complexity of such a search operation is linear with respect to the duration of the search interval.

3.1.2 Slowly Varying $\mathbf{S_z(f)}$

Assuming that $S_z(f) \cong S_z(f_k) = N_0 + S_I(f_k)$ for $|f - f_k| \leq \Delta/2 \ \forall k$, $\rho_{k,k}$ in (3.14) becomes

$$\begin{aligned} \rho_{k,k} &= w_k \int\limits_{f_k - \Delta/2}^{f_k + \Delta/2} |P(f - f_k)|^2 \, |H(f)|^2 \, \mathrm{d}f \\ &= w_k \int\limits_{f_k - \Delta/2}^{f_k + \Delta/2} \frac{|P(f - f_k)|^2}{S_z(f)} \mathrm{d}f \\ &\cong \frac{w_k}{S_z(f_k)} \int\limits_{f_k - \Delta/2}^{f_k + \Delta/2} |P(f - f_k)|^2 \, \mathrm{d}f \\ &= \frac{w_k}{S_z(f_k)} \int\limits_{-\Delta/2}^{\Delta/2} |P(f)|^2 \, \mathrm{d}f \\ &= \frac{w_k \, E_p}{S_z(f_k)} \ , \end{aligned} \tag{3.16}$$

which can be substituted into $\hat{\tau}$ in (3.15) to obtain

$$\begin{aligned}\hat{\tau} &= \arg\max_{\tilde{\tau}} \left\{ \sum_{\substack{k=1\\ \rho_{k,k}\neq 0}}^{K} \rho_{k,k}^{-1} \left|x_k\left(\tilde{\tau}\right)\right|^2 \right\} \\ &= \arg\max_{\tilde{\tau}} \left\{ \frac{1}{E_p} \sum_{\substack{k=1\\ w_k\neq 0}}^{K} \frac{S_z(f_k)}{w_k} \left|x_k\left(\tilde{\tau}\right)\right|^2 \right\} \\ &= \arg\max_{\tilde{\tau}} \left\{ \sum_{\substack{k=1\\ w_k\neq 0}}^{K} \frac{S_z(f_k)}{w_k} \left|x_k\left(\tilde{\tau}\right)\right|^2 \right\}. \end{aligned} \tag{3.17}$$

3.2 Numerical Examples

In this section, numerical examples, that illustrate the impact of the optimal weight selection on the CRBs and ML TOA estimation in the absence and presence of interference, are provided. Simulation results of two scenarios involving two different pulse shapes are presented to support the theoretical analysis.

3.2.1 Gaussian Pulse

A scenario with subcarrier spacing $\Delta = 10$ MHz and $K = 128$ is considered. The channel coefficients α_k are modeled as independent complex-valued Gaussian random variables with unit average power, and the results are obtained by averaging over 500 independent channel realizations. The pulse $p(t)$ in (2.1) is modeled as a Gaussian doublet, expressed by

$$p(t) = A\left(1 - \frac{4\pi\, t^2}{\zeta^2}\right) e^{-\frac{2\pi\, t^2}{\zeta^2}}\ , \tag{3.18}$$

with $A = \sqrt{\frac{8E_p}{3\zeta}}$, where E_p is the pulse energy and parameter ζ serves to adjust the pulse width. In experiments, ζ is chosen to be $0.4\,\mu$s, which corresponds to a pulse width of about 1 μs. Parameters β_1 and β_2 in (2.28) are $\beta_1 = 0$

and $\beta_2 = \frac{5}{2\pi\zeta^2}$, respectively. The following results are expressed in terms of the square-root of the CRB for TOA, multiplied by the speed of light.

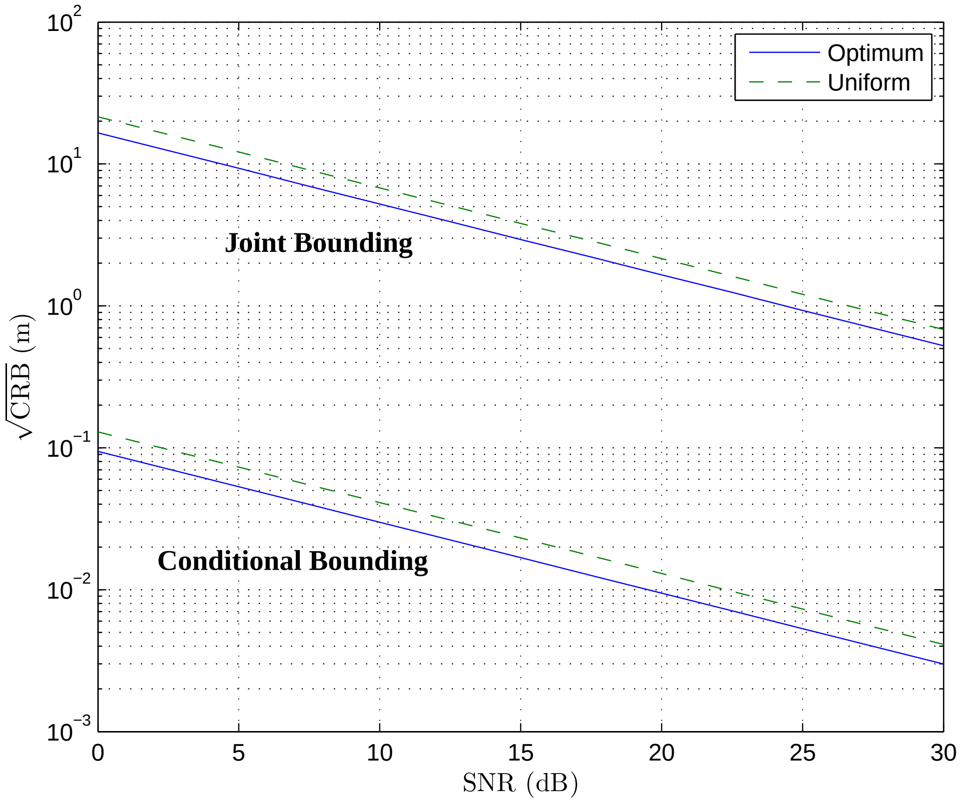

Figure 3.1: $\sqrt{\mathrm{CRB}}$ versus SNR for optimal and conventional algorithm in the absence of interference.

Figure 3.1 illustrates $\sqrt{\mathrm{CRB}}$ (in meters) versus the signal-to-noise ratio (SNR) in the absence of interference for the optimal algorithm (with weights computed from (2.39)) and for a conventional algorithm that assigns equal weights to the subcarriers (uniform) in the cases of joint and conditional bounding described in Section 2.2.1 and Section 2.2.2, respectively. The SNR is defined as $\mathrm{SNR} = E_p/N_0$. It is assumed that w_k can not exceed $2/K$, i.e., $b_k = 2/K$ for $k = 1, \ldots, K$. It is seen that a gain of about 3 dB in terms of SNR is obtained with the optimal weights in both cases. In addition, the bounds obtained from conditional bounding are observed to be very low (optimistic), since that technique assumes knowledge of the channel coefficients. Therefore, the following results consider only the joint bounding.

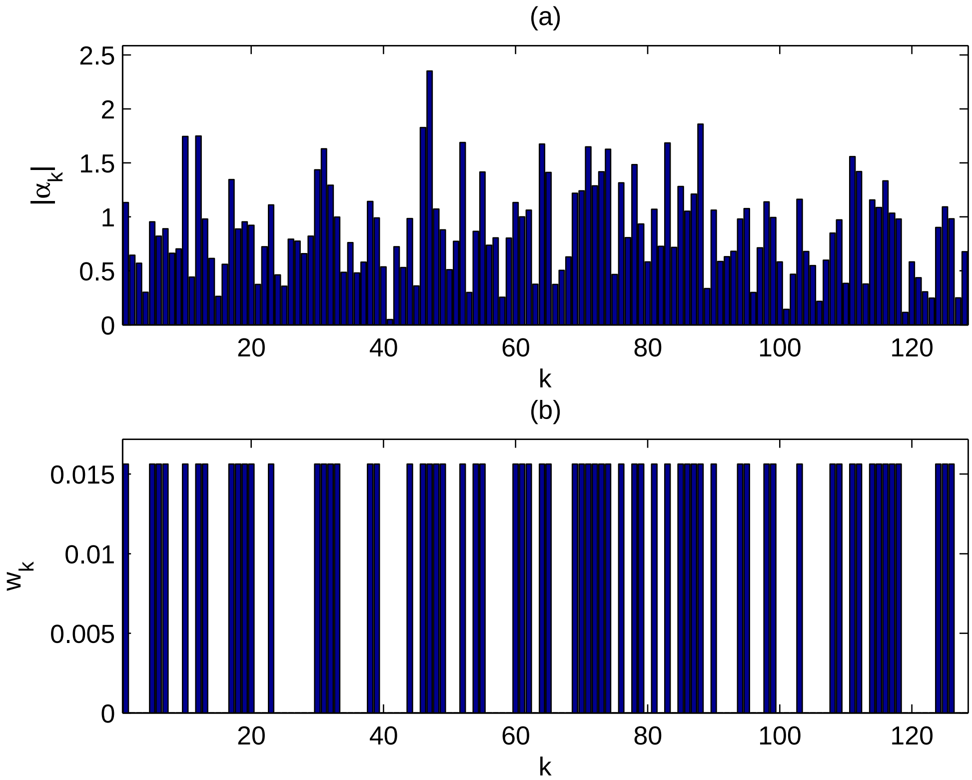

Figure 3.2: (a) Channel amplitudes versus subcarrier index. (b) Optimal weights versus subcarrier index.

Figure 3.2 shows a realization of the channel coefficients and the corresponding optimal weights in the absence of interference. As expected, the subcarriers with larger channel amplitudes are favored.

Next, we consider the effects of interference. All the system parameters are as before, but $S_I(f)$ now takes a constant value $2N_0$ for subcarrier indices k between 33 and 96 and it is zero elsewhere. In Figure 3.3, the square-root of the CRB is plotted against SNR for two different scenarios. In the first one, an interference avoidance strategy is adopted where the transmitted signal has no power at the subcarriers with interference, i.e., for $33 \leq k \leq 96$, while in the second, all the subcarriers can be potentially employed. In both cases, the conventional

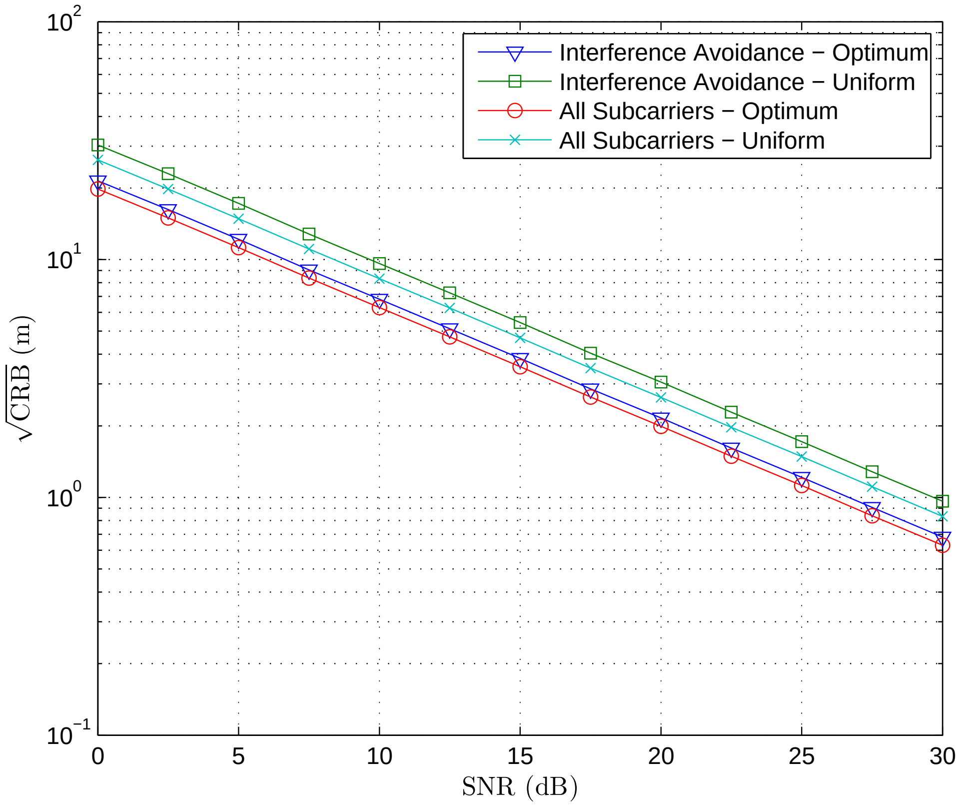

Figure 3.3: $\sqrt{\mathrm{CRB}}$ versus SNR for the optimal and conventional (uniform) algorithm in the presence of interference with a flat spectral density in the interval $33 \leq k \leq 96$.

(uniform) and the optimal algorithm are examined. It can be realized that using all the subcarriers reduces the CRB with respect to the interference avoidance strategy. However, the improvement becomes insignificant as the number of subcarriers affected by the interference gets small and/or the interference power increases. This is seen in Figure 3.4, which shows the square-root of the CRB when the interference spectrum extends from subcarrier 49 to subcarrier 80 with a spectral density of $4N_0$.

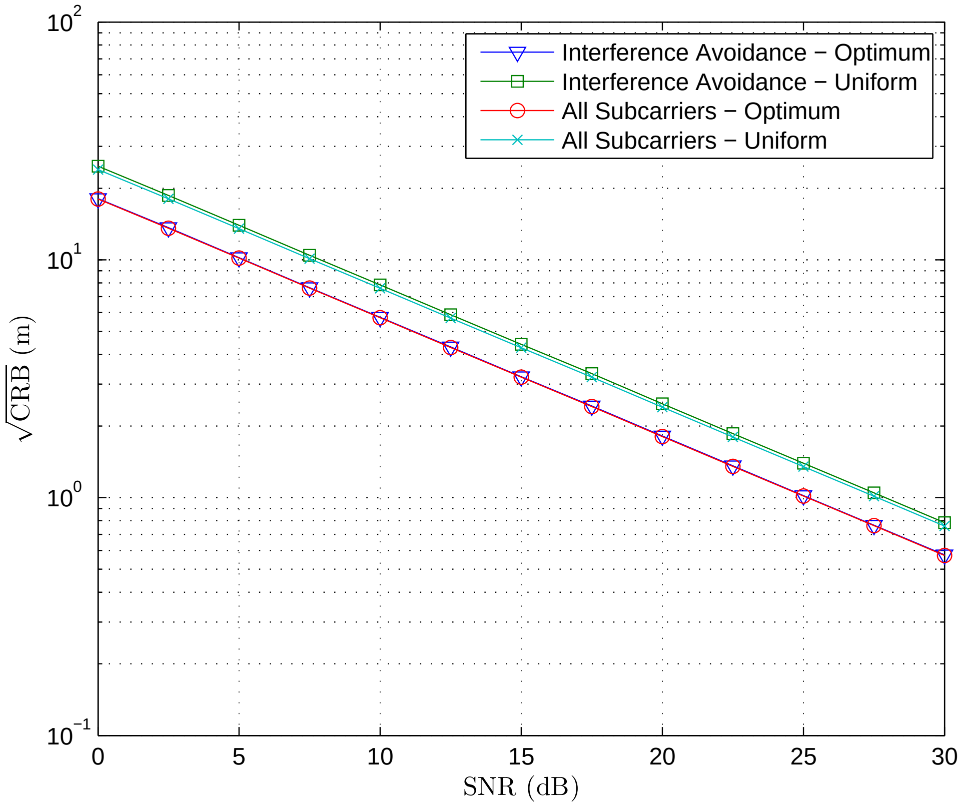

Figure 3.4: $\sqrt{\text{CRB}}$ versus SNR for the optimal and conventional (uniform) algorithm in the presence of interference with a flat spectral density in the interval $49 \leq k \leq 80$.

Figure 3.5 illustrates the subcarrier coefficients λ_k in (2.30) and the corresponding optimal weight distribution in two scenarios: One uses only the interference-free subcarriers (interference avoidance), whereas the other employs all the subcarriers. As noted from (2.39), the subcarriers with large λ_k are favored in the optimal spectrum.

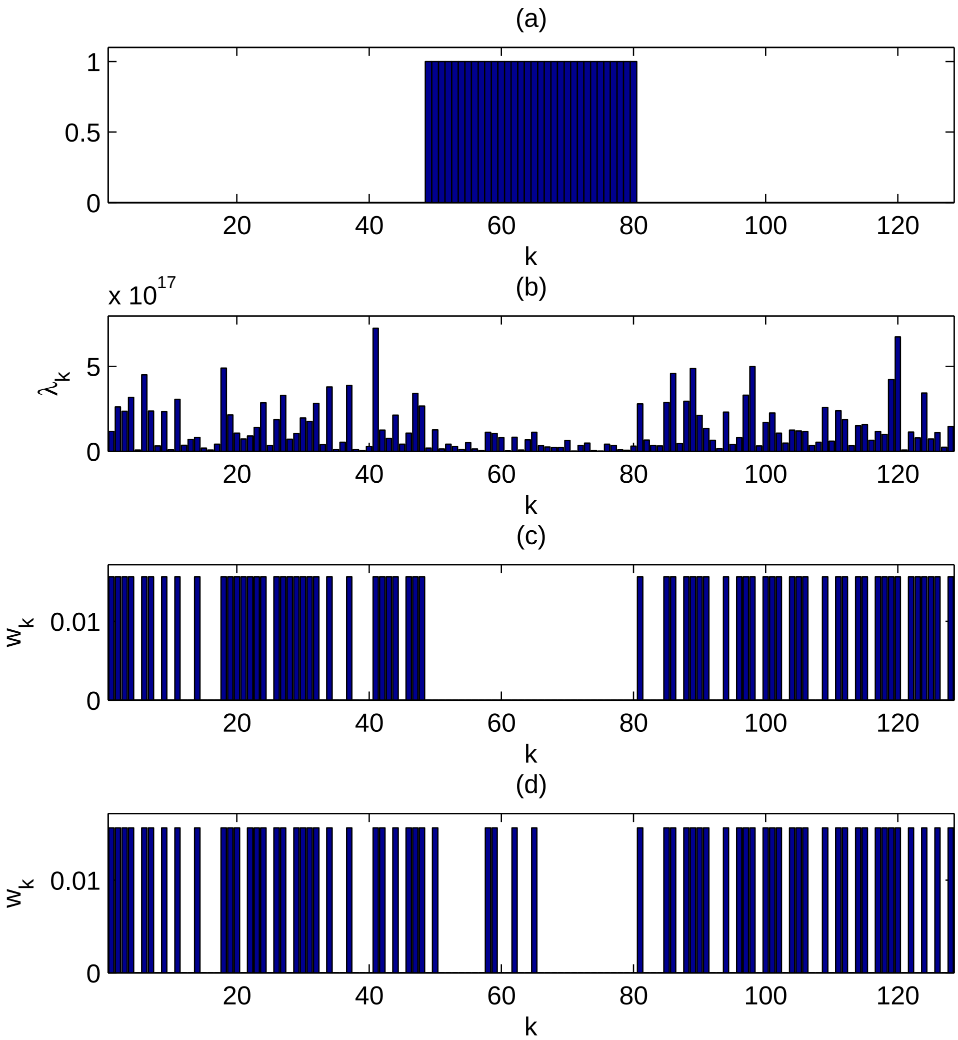

Figure 3.5: (a) Spectrum of the interference. (b) Subcarrier coefficient λ_k versus subcarrier index k. (c) Subcarrier weights versus subcarrier index for the optimal algorithm that uses only the interference-free subcarriers (interference avoidance). (d) Subcarrier weights versus subcarrier index for the optimal algorithm that uses all the subcarriers.

3.2.2 Sinc Pulse

A scenario with subcarrier spacing $\Delta = 1$ MHz and $K = 128$ subcarriers is considered. The channel coefficients α_k are modeled as independent complex-valued Gaussian random variables with unit average power. The results are obtained by averaging over 500 independent channel realizations. Pulse $p(t)$ in (2.1) is modeled as a sinc pulse; namely,

$$p(t) = \sqrt{E_p\Delta}\,\mathrm{sinc}(\Delta \mathrm{t}) = \sqrt{\mathrm{E_p}\Delta}\,\frac{\sin(\pi \mathrm{t}\Delta)}{(\pi \mathrm{t}\Delta)}. \tag{3.19}$$

Parameters β_1 and β_2 in (2.28) are set to 0 and $\Delta^2/12$, respectively. The results are expressed in terms of the square-root of the CRB on the *ranging error*, which is computed as the product of the square-root of the CRB on TOA error multiplied by the speed of light.

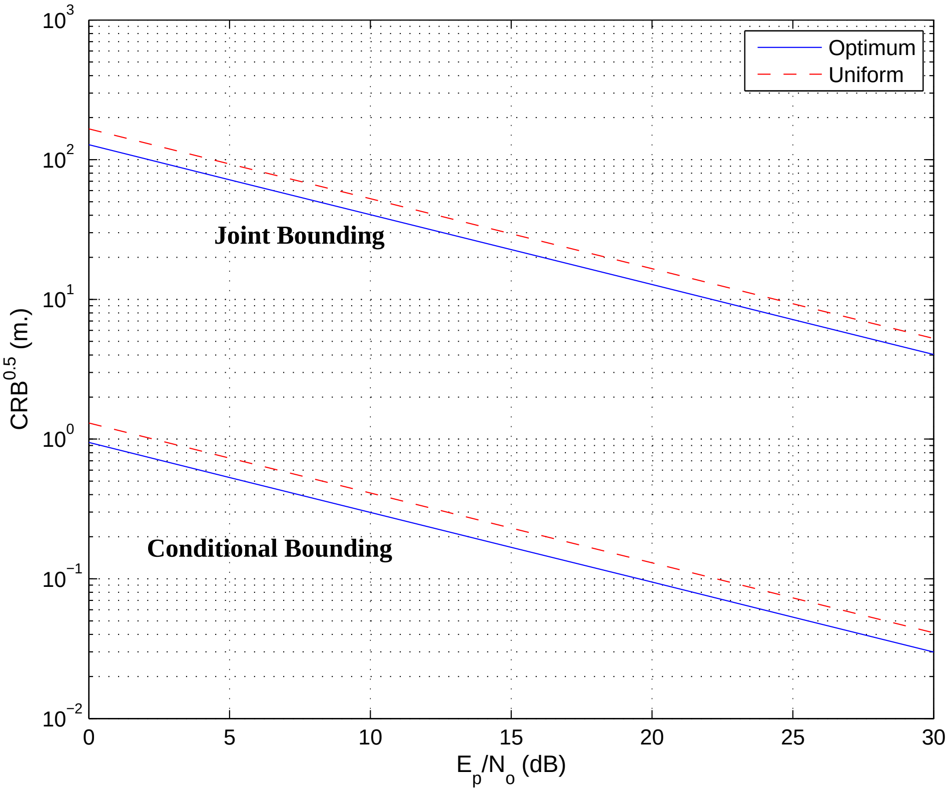

Figure 3.6: $\sqrt{\mathrm{CRB}}$ versus E_p/N_0 for optimal and conventional (uniform) algorithm in the absence of interference.

In Figure 3.6 the square-root of the CRB (in meters) is plotted against E_p/N_0 in the absence of interference for the optimal algorithm (whose weights are computed from (2.39)) and for the conventional algorithm that assigns equal weights to the subcarriers (uniform). It is assumed that w_k can not exceed $2/K$, which implies that the power constraint defined in Section 2.3 is specified by $b_k = 2/K$ for $k = 1, \ldots, K$. Both joint and conditional bounds are drawn (see Sections 2.2.1 and 2.2.2). The figure shows that a gain of about 3 dB in terms of E_p/N_0 is obtained with the optimal weights. However, the conditional bounding gives very low (optimistic) results compared with the joint bounding for it assumes knowledge of the channel gains. Henceforth, we concentrate on joint bounding.

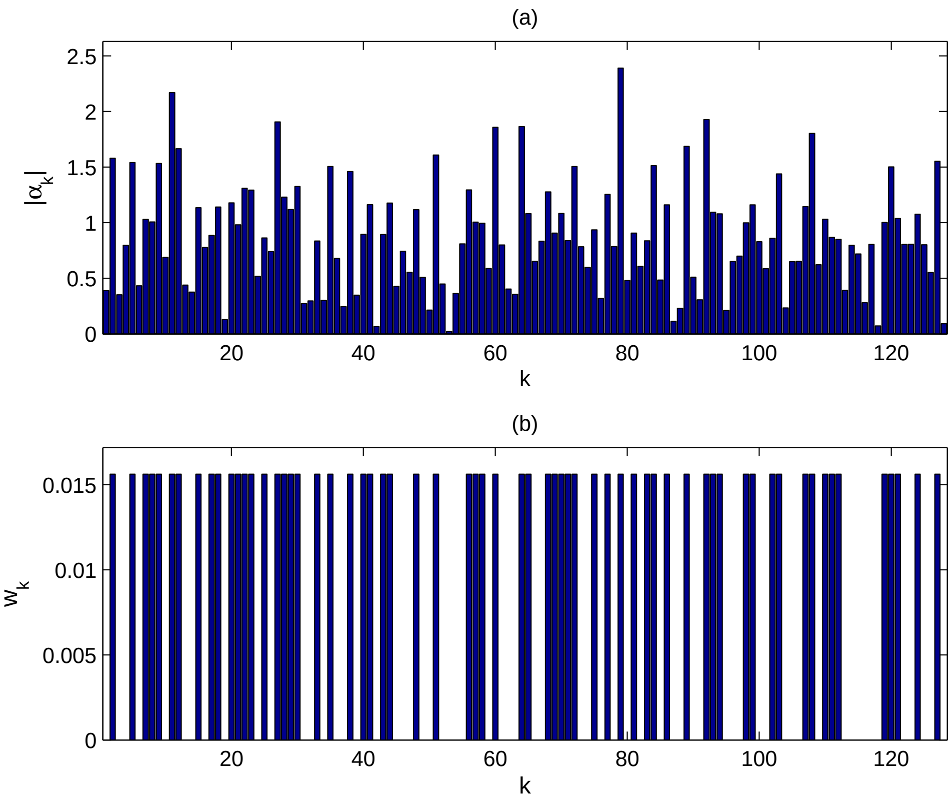

Figure 3.7: (a) Channel amplitudes versus subcarrier index. (b) Optimal weights versus subcarrier index.

Figure 3.7 shows a realization of the channel coefficients and the corresponding optimal weights in the absence of interference. As expected from (2.39), the subcarriers with larger channel amplitudes are favored.

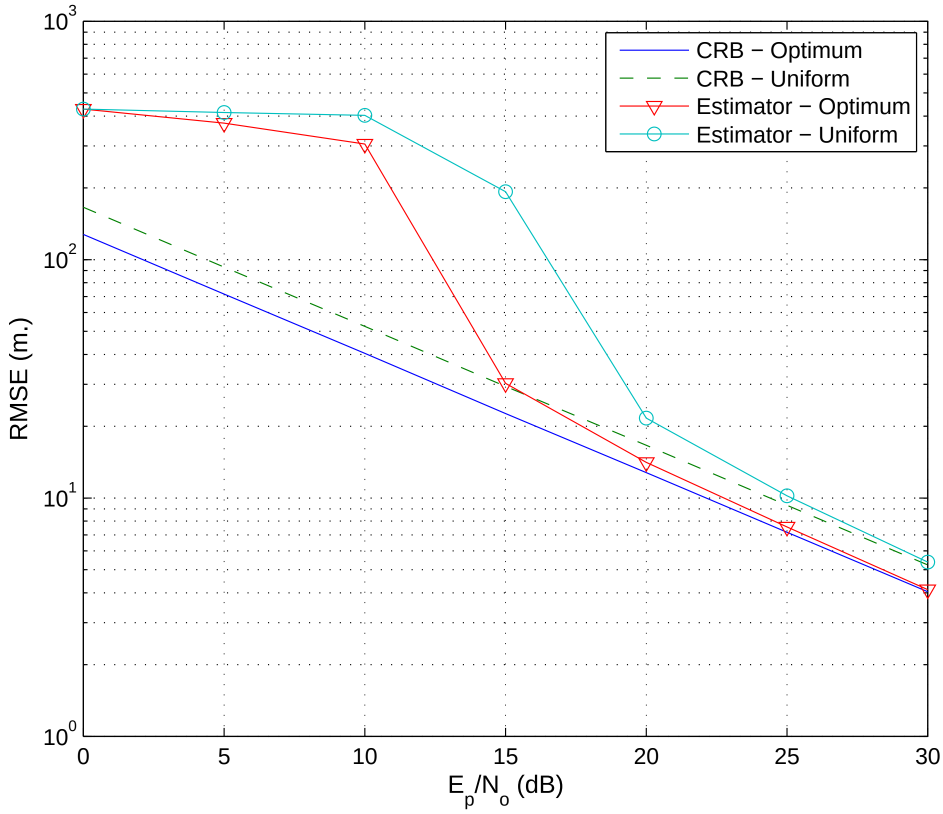

Figure 3.8: RMSE versus E_p/N_0 for the practical TOA estimation algorithms based on optimal and uniform weight assignments. Also, the CRBs are illustrated for both cases. No interference is assumed in this scenario.

Next, the performance of the ML TOA estimator in (3.15) is investigated for optimal and uniform weight assignments. The aim is to see whether the optimal weight assignment, which is based on the CRB minimization, is also effective in practical TOA estimators. In Figure 3.8, the root-mean-squared error (RMSE) of the ML TOA estimator is shown with optimal and uniform weights and is compared with the corresponding CRBs. It is observed that the optimal weights also improve the performance of the ML TOA estimator.

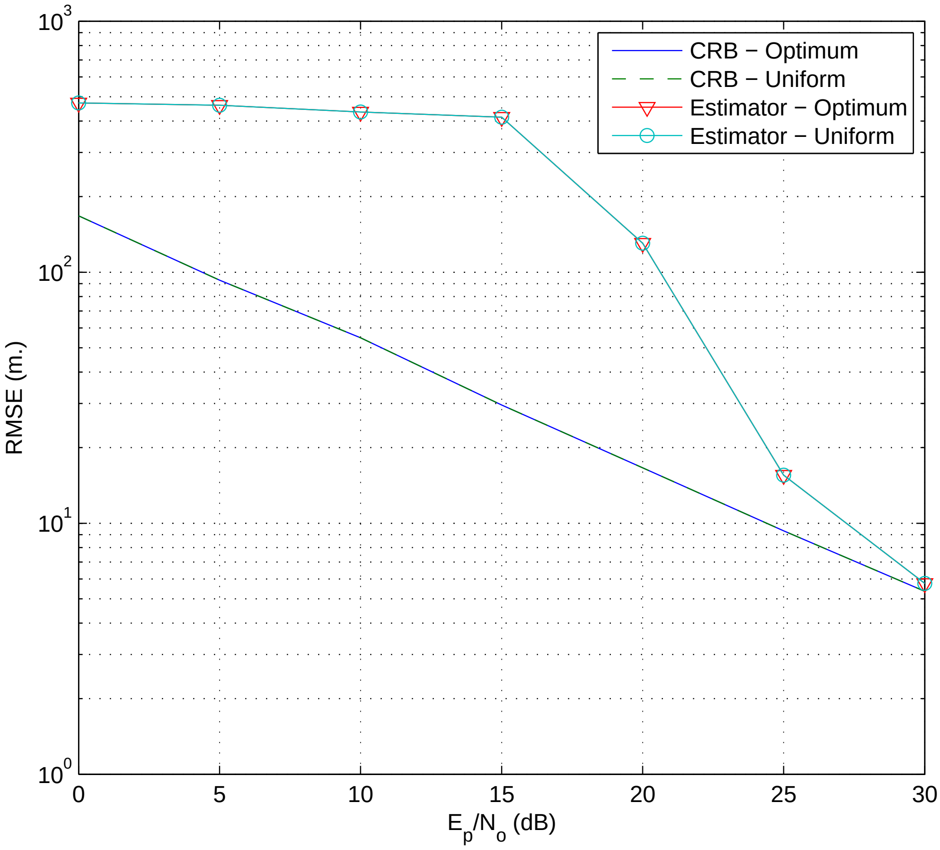

Figure 3.9: RMSE versus E_p/N_0 for the optimal and conventional (uniform) algorithms in the presence of interference with a flat spectral density in the interval $23 \leq k \leq 106$. In this scenario, the subcarriers with interference are not used (interference avoidance).

Now we concentrate on the effects of interference. The system parameters are all as before. The interference spectral density $S_I(f)$ takes a constant value of $N_I = 2N_0$ for the subcarrier indices from 23 to 106 while it is zero elsewhere. In Figure 3.9 the performance of the ML TOA estimator and the CRB are illustrated with optimal and conventional (uniform) weights in the case of an interference avoidance strategy. This means that the transmitted power is set to zero at the subcarriers with interference (i.e., $w_k = 0$ for $23 \leq k \leq 106$) while uniform and optimal power allocation is used for the remaining subcarriers. Unlike Figure 3.8, it is observed that the optimal and uniform allocation strategies provide the same TOA estimation accuracy in this case. In addition, it is seen that the estimation errors increase significantly in the presence of interference when the subcarriers with interference are not utilized.

In Figure 3.10 the same scenario is considered except that all the subcarriers can now be employed. In this case, it is observed that the optimal algorithm improves both the CRB and the TOA estimation accuracy of the ML algorithm compared to the conventional (uniform) algorithm. In addition, the mean error values are smaller than those in the interference avoidance case, as expected (cf. Figure 3.9).[1] We conclude that subcarriers with interference should be employed to better utilize the frequency diversity and enhance TOA estimation performance.

In order to explain the mechanisms behind the results in Figures 3.9 and 3.10, Figure 3.11 illustrates a realization of the channel coefficients and the corresponding optimal weights according to both the interference avoidance strategy (Figure 3.11-(c)) and the strategy that uses all the subcarriers (Figure 3.11-(d)) at $E_p/N_0 = 30\,\text{dB}$. Since the interference-free subcarriers are few in the considered scenario, all the subcarriers are used in the interference avoidance case (see

[1]For the sake of fairness it should be noted that the transmitted signal powers (see (2.2)) are not the same in Figs. 4 and 5 due to the power constraint, $2/K$. Specifically, in the former $\sum_{k=1}^{K} w_k$ equals $\frac{2}{128} \times 44 = 0.6875$ while in the latter it is unity.

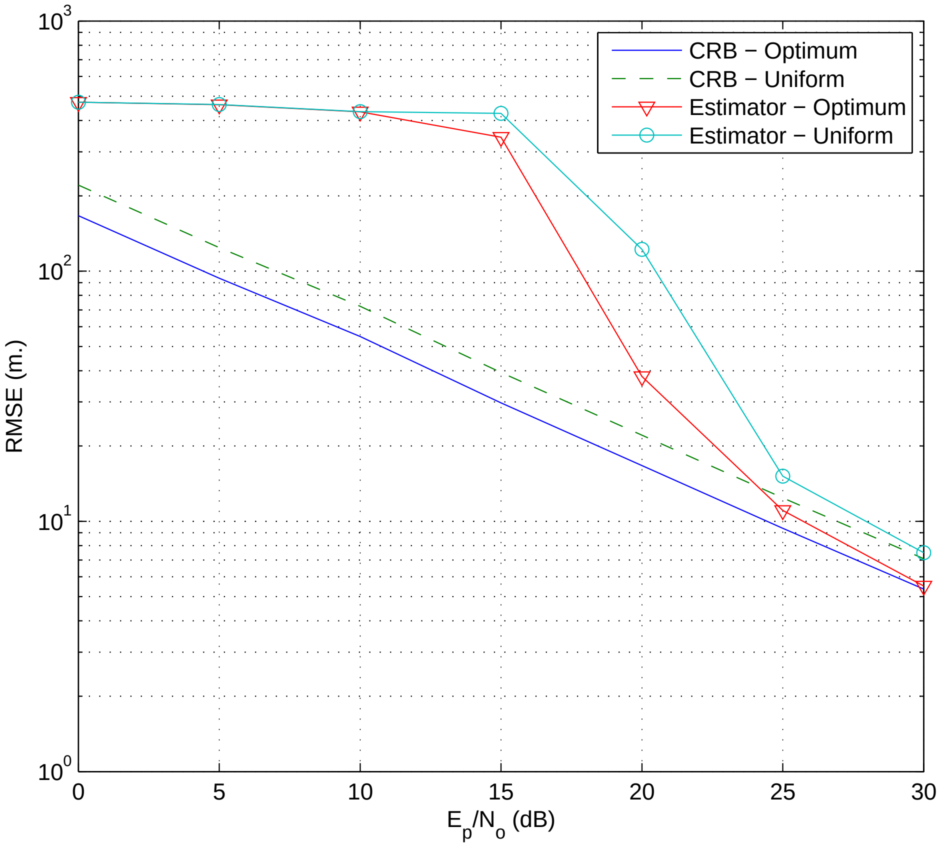

Figure 3.10: RMSE versus E_p/N_0 for the optimal and conventional (uniform) algorithms in the presence of interference with a flat spectral density in the interval $23 \leq k \leq 106$. In this scenario, the subcarriers with interference are also used.

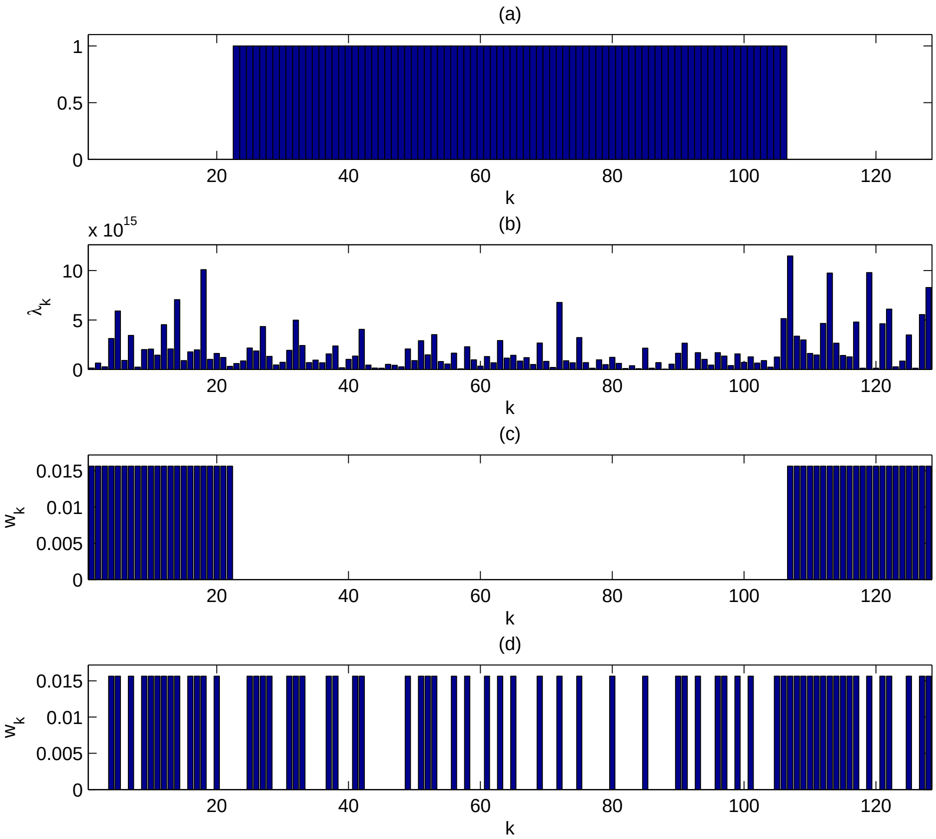

Figure 3.11: (a) Spectrum of the interference. (b) Subcarrier coefficient λ_k versus subcarrier index k. (c) Subcarrier weights versus subcarrier index for the optimal algorithm that uses only the interference-free subcarriers (interference avoidance). (d) Subcarrier weights versus subcarrier index for the optimal algorithm that uses all the subcarriers.

Figure 3.14 for a different situation) . Therefore, the optimal algorithm assigns the maximum allowed power to all the interference-free subcarriers and, in so doing, its performance becomes identical to that uniform algorithm as seen in Figure 3.9. Figure 3.11-(d) indicates that, if all the subcarriers can be used, some interfered subcarriers can be chosen instead of interference-free ones, depending on the channel amplitudes. Correspondingly, the optimal power allocation algorithm provides improved TOA estimation performance compared to the uniform algorithm, as can be seen in Figure 3.10.

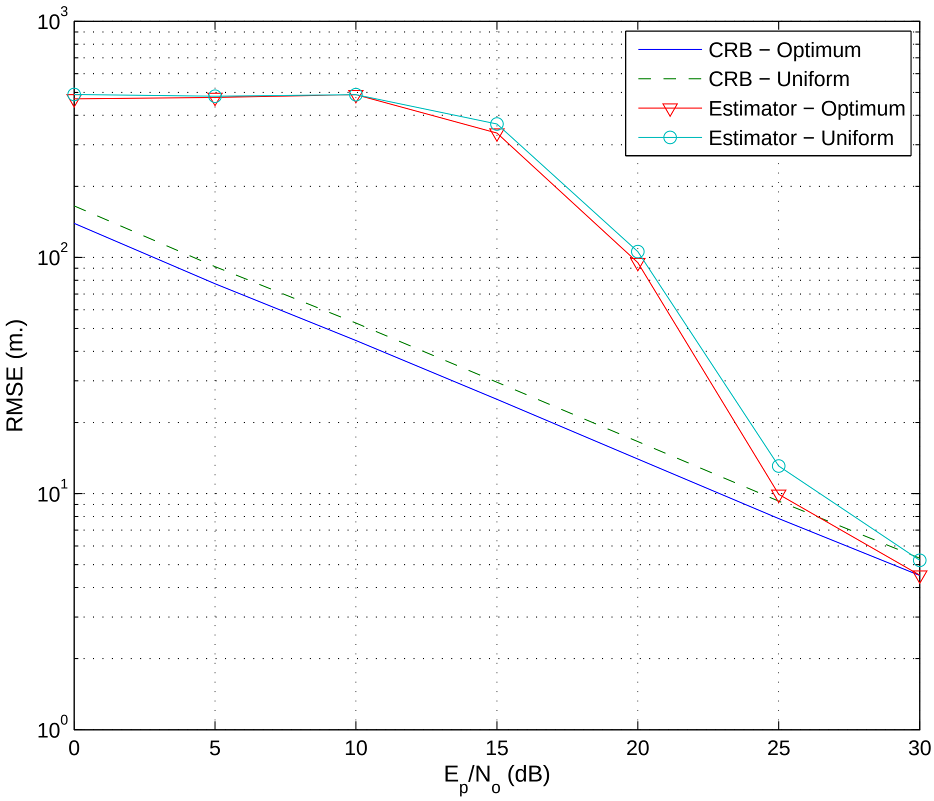

Figure 3.12: RMSE versus E_p/N_0 for the optimal and conventional (uniform) algorithms in the presence of interference with a flat spectral density of $4N_0$ in the interval $49 \leq k \leq 80$. In this scenario, the subcarriers with interference are not used (interference avoidance).

The improvement achievable by using all the subcarriers (instead of the interference-free ones only) depends on the interference power and the number of subcarriers with interference. Specifically, the improvement reduces as the

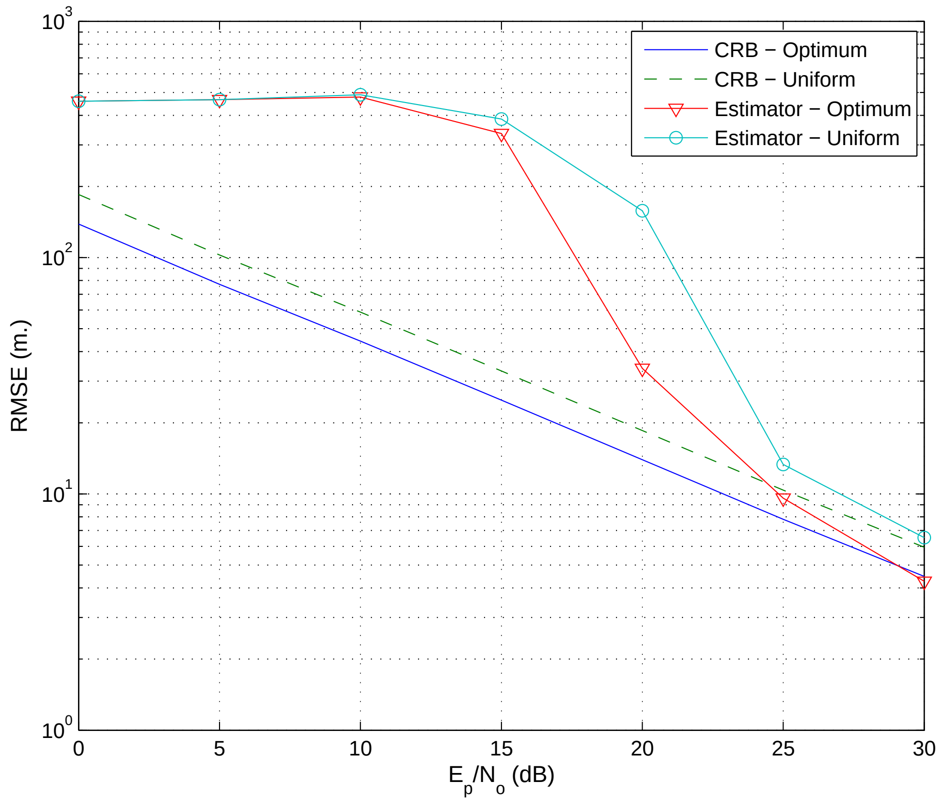

Figure 3.13: RMSE versus E_p/N_0 for the optimal and conventional (uniform) algorithms in the presence of interference with a flat spectral density of $4N_0$ in the interval $49 \leq k \leq 80$. In this scenario, the subcarriers with interference are also used.

number of subcarriers with interference decreases, and/or the interference power increases. Figures 3.12 and 3.13 show the CRB and the performance of the ML TOA estimator for interference-avoidance and no-avoidance cases, respectively, when the interference spectrum extends from subcarrier 49 to subcarrier 80 with a spectral density of $N_I = 4N_0$. We recognize that the gain achieved by exploiting all the subcarriers is less significant compared with the scenarios discussed in Figures 3.9 and 3.10. Still, a significant advantage is obtained with the optimal weights in place of the conventional ones.

In addition, Figure 3.14 illustrates the subcarrier coefficients λ_k in (2.30) and the corresponding optimal weights at $E_p/N_0 = 30\,\text{dB}$ in two cases: one using only the interference-free subcarriers (interference avoidance), the other employing all the subcarriers. In agreement with (2.39) we see that the subcarriers with larger λ_k's and/or smaller interference are favored in the optimal spectrum.

Figures 3.15 and 3.16 illustrate how the power of interference dynamically affects the CRB and the performance of the ML TOA estimator through the signal-to-interference ratio (SIR). An increase in the interference spectral density results in an increase in the RMSE of the ML TOA estimator while the corresponding CRB is not influenced significantly since only one-fourth of the subcarriers experience interference. It is also observed that, as the interference power decreases, the gain from the utilization of the optimal power allocation scheme increases in both scenarios.

Finally, the performance sensitivity of the CRB and the ML TOA estimators to spectral estimation errors is investigated. It is assumed that interference spectral density $S_I(f)$ takes a constant value of $N_I = 4N_0$ for the subcarrier indices from 23 to 106 while it is zero elsewhere. Assuming that the spectral estimation error can be modeled as a zero-mean Gaussian random variable with variance σ_e^2, Table 3.1 presents RMSE values of the ML TOA estimators and the CRBs for the optimal and uniform power allocation strategies for various

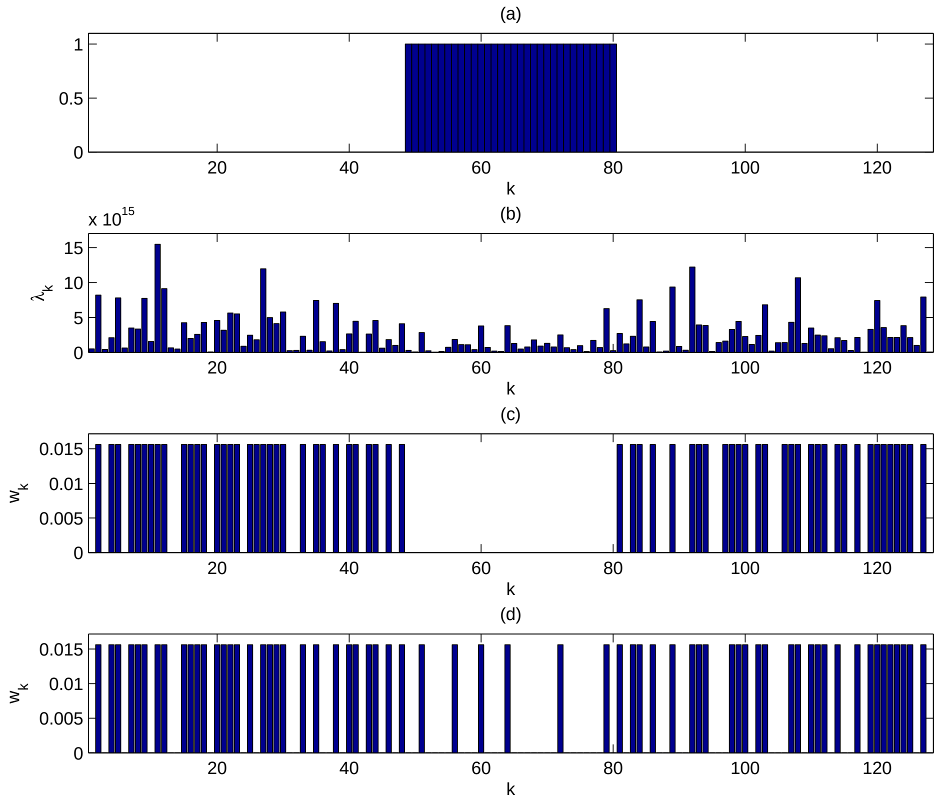

Figure 3.14: (a) Spectrum of the interference. (b) Subcarrier coefficient λ_k versus subcarrier index k. (c) Subcarrier weights versus subcarrier index for the optimal algorithm that uses only the interference-free subcarriers (interference avoidance). (d) Subcarrier weights versus subcarrier index for the optimal algorithm that uses all the subcarriers.

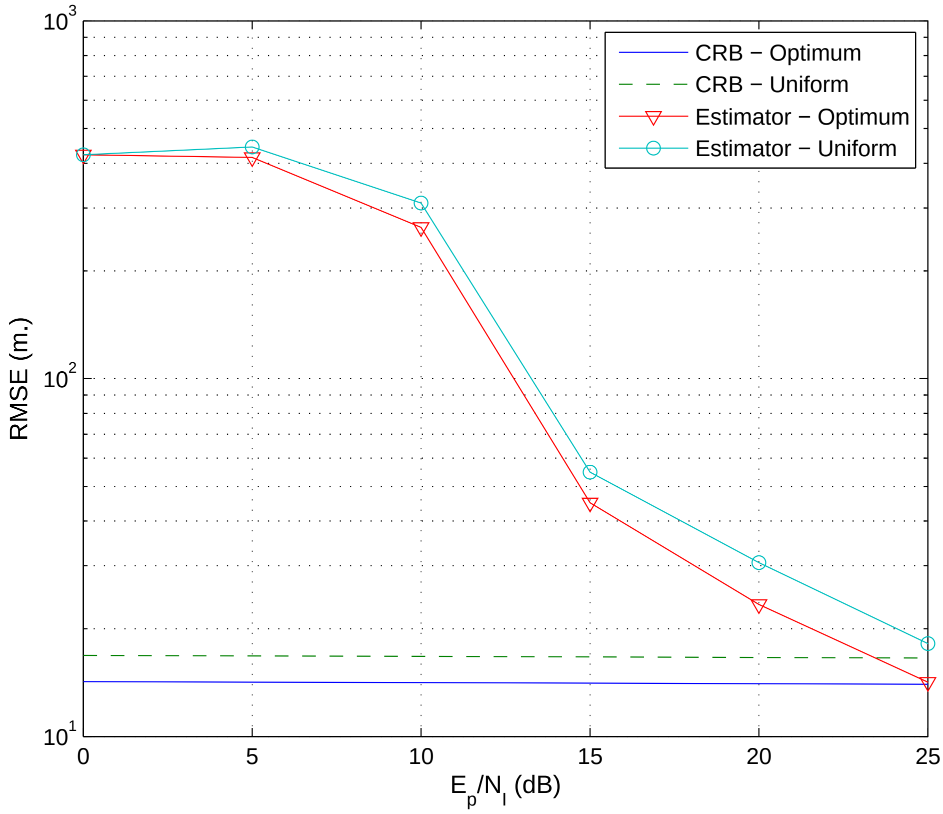

Figure 3.15: RMSE versus SIR (defined as E_p/N_I) for the optimal and conventional (uniform) algorithms in the presence of interference in the interval $49 \leq k \leq 80$, where $E_p/N_0 = 20\,\text{dB}$. In this scenario, the subcarriers with interference are not used (interference avoidance).

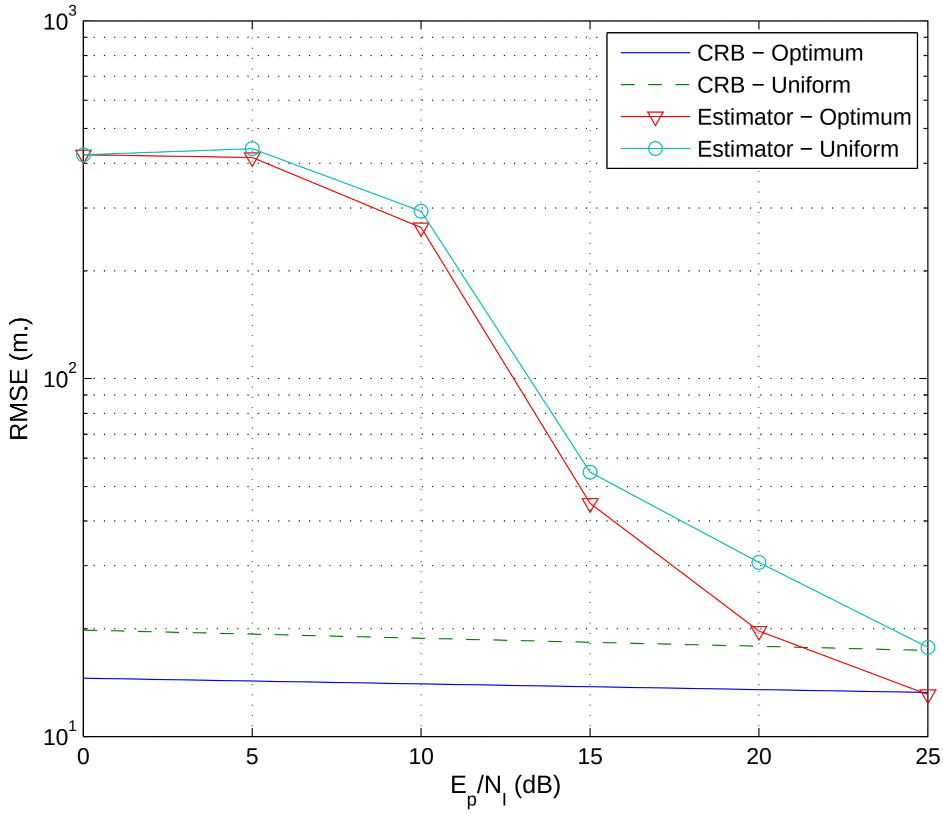

Figure 3.16: RMSE versus SIR (defined as E_p/N_I) for the optimal and conventional (uniform) algorithms in the presence of interference in the interval $49 \leq k \leq 80$, where $E_p/N_0 = 20\,\text{dB}$. In this scenario, the subcarriers with interference are also used.

spectral estimation error variances at $E_p/N_0 = 30\,\mathrm{dB}$ for the scenario in which all the subcarriers are used. It is observed that an increase in the uncertainty of spectral estimation (that is, σ_e^2) leads to an increase in the CRB and the RMSE of the ML TOA estimator for the optimal power allocation strategy. On the other hand, when the uniform power allocation strategy is used, the performance is not affected from the spectral estimation errors. The reason for this is that the optimal power allocation strategy uses the knowledge of the interference level whereas the uniform one always assigns equal powers to all the subcarriers irrespective of the interference level. Although the optimal power allocation strategy is influenced adversely by the spectral estimation errors, it is also noted that its performance is consistently superior to that of the uniform power allocation strategy even for substantially high values of spectral estimation errors. This demonstrates the robustness of the optimal power allocation scheme against uncertainties in the spectral estimation mechanism of a CR system.

	$\sigma_e^2 = 0$	$\sigma_e^2 = 0.5$	$\sigma_e^2 = 1$	$\sigma_e^2 = 1.5$
Estimator - Optimal	8.402	8.565	8.622	8.720
Estimator - Uniform	10.58	10.58	10.58	10.58
$\sqrt{\mathrm{CRB}}$ - Optimal	5.611	5.681	5.718	5.750
$\sqrt{\mathrm{CRB}}$ - Uniform	7.617	7.617	7.617	7.617

Table 3.1: RMSE (in meters) versus spectrum estimation error variance, σ_e^2.

Chapter 4

Conclusions and Future Work

In this thesis, theoretical limits on TOA estimation have been studied in the context of CR systems. Specifically, closed form CRB expressions have been obtained for TOA estimation in the presence of interference in OFDM-based CR systems under a wide variety of practical scenarios. Based on CRB expressions, an optimal power allocation (or, spectrum shaping) strategy, that offers the best possible TOA estimation accuracy, has been proposed. The proposed power allocation scheme also takes the constraints imposed by the regulatory emission mask and the sensed interference spectrum into consideration. Then, ML TOA estimator has been derived for OFDM-based signalling scheme and its performance is investigated against the theoretical limits offered by the CRB expressions. Numerical results for the CRBs and ML TOA estimator have been obtained and the effects of the optimal power allocation on the accuracy of ML TOA estimator have been investigated in the absence/presence of interference. The use of optimal power allocation strategy instead of the conventional uniform power assignment scheme has been demonstrated to bring in significant gains in terms of TOA estimation accuracy. It has also been observed that the intuitive interference avoidance strategy, which assigns signal power only to the interference-free subcarriers, is not optimal when compared with optimal power allocation that utilizes all subcarriers in power assignment. In other words, the frequency diversity can be utilized more efficiently if all the subcarriers, including the ones with interference, are employed for TOA estimation. Finally, analysis of the performance sensitivity of the optimal power allocation strategy to the uncertainty in spectrum estimation has been carried out, and the performance of optimal power allocation has been shown to be consistently superior to that of the uniform allocation even for substantially high values of spectral estimation errors.

Future work will be focused on obtaining closed form CRB expressions for multiple input multiple output (MIMO) systems employing the OFDM-based signalling scheme examined in this thesis. In case the MIMO-OFDM system results in complicated CRB expressions that are not possible to be expressed in closed forms, numerical analysis can be resorted to evaluate the effectiveness of the proposed optimal power allocation strategy. The ML TOA estimator derived for the single input single output (SISO) system in the presence of interference should also be modified in a way to take the spatial diversity offered by MIMO systems into consideration.

APPENDIX A

Proofs and Derivations

A.1 Log-likelihood function in (2.7)

The likelihood function at the output of the whitening filter $h(t)$ can be written as [38]

$$\bar{\Lambda}(\widetilde{\boldsymbol{\theta}}) = exp\left\{-\int_{-\infty}^{\infty}\left|x(t)-u(t,\widetilde{\boldsymbol{\theta}})\right|^{2}\mathrm{d}t\right\}\ , \tag{A.1}$$

where the interference plus noise power spectral density $S_z(f)$ is taken to be unity since the total disturbance z(t) is already whitened. Expanding the term inside the curly braces, we get

$$\bar{\Lambda}(\widetilde{\boldsymbol{\theta}}) = exp\left\{-\int_{-\infty}^{\infty}|x(t)|^{2}\,\mathrm{d}t + 2\,\Re\left\{\int_{-\infty}^{\infty}x(t)u^{*}(t,\widetilde{\boldsymbol{\theta}})\right\} - \int_{-\infty}^{\infty}\left|u(t,\widetilde{\boldsymbol{\theta}})\right|^{2}\mathrm{d}t\right\}\ . \tag{A.2}$$

Note that the first term inside the exponent of (A.2) does not involve the channel parameter vector $\widetilde{\boldsymbol{\theta}} = [\tau\ a_1 \cdots a_K\ \phi_1 \cdots \phi_K]$ to be estimated, and hence it can be neglected in finding the estimate $\hat{\boldsymbol{\theta}}$ that maximizes the likelihood function. Dividing rest of the exponent by 2 yields the following equivalent likelihood function

$$\Lambda(\widetilde{\boldsymbol{\theta}}) = exp\left\{\Re\left\{\int\limits_{-\infty}^{\infty} x(t)u^*(t,\widetilde{\boldsymbol{\theta}})\mathrm{d}t\right\} - \frac{1}{2}\int\limits_{-\infty}^{\infty}\left|u(t,\widetilde{\boldsymbol{\theta}})\right|^2\mathrm{d}t\right\}, \tag{A.3}$$

since taking the square root of an always positive objective function has no effect on the maximizing parameter value. From (A.3), the corresponding log-likelihood function can be written as

$$\ln\Lambda(\widetilde{\boldsymbol{\theta}}) = \Re\left\{\int\limits_{-\infty}^{\infty} x(t)u^*(t,\widetilde{\boldsymbol{\theta}})\mathrm{d}t\right\} - \frac{1}{2}\int\limits_{-\infty}^{\infty}\left|u(t,\widetilde{\boldsymbol{\theta}})\right|^2\mathrm{d}t. \tag{A.4}$$

A.2 Log-likelihood function in (2.10)

Substitution of

$$x(t) = r(t)\otimes h(t) = \int\limits_{-\infty}^{\infty} r(z)h(t-z)\mathrm{d}z \tag{A.5}$$

and

$$u(t,\widetilde{\boldsymbol{\theta}}) = \tilde{s}_r(t-\tilde{\tau})\otimes h(t) = \int\limits_{-\infty}^{\infty}\tilde{s}_r(z-\tilde{\tau})h(t-z)\mathrm{d}z \tag{A.6}$$

into the log-likelihood function in (2.7) gives

$$\begin{aligned}\ln\Lambda(\widetilde{\boldsymbol{\theta}}) = \Re&\left\{\int\limits_{-\infty}^{\infty}\int\limits_{-\infty}^{\infty} r(z)h(t-z)\mathrm{d}z\int\limits_{-\infty}^{\infty}\tilde{s}_r^*(v-\tilde{\tau})h^*(t-v)\mathrm{d}v\,\mathrm{d}t\right\} - \\ &\left\{\frac{1}{2}\int\limits_{-\infty}^{\infty}\int\limits_{-\infty}^{\infty}\tilde{s}_r(z-\tilde{\tau})h(t-z)\mathrm{d}z\int\limits_{-\infty}^{\infty}\tilde{s}_r^*(v-\tilde{\tau})h^*(t-v)\mathrm{d}v\,\mathrm{d}t\right\}.\end{aligned} \tag{A.7}$$

Defining a new function

$$Q(z,v) \triangleq \int\limits_{-\infty}^{\infty} h(t-z)h^*(t-v)\mathrm{d}t = \int\limits_{-\infty}^{\infty} h(t)h^*(t-v+z)\mathrm{d}t \tag{A.8}$$

leads to the following expression for log-likelihood function

$$\begin{aligned}\ln\Lambda(\widetilde{\boldsymbol{\theta}}) = \Re&\left\{\int\limits_{-\infty}^{\infty} r(z)\int\limits_{-\infty}^{\infty} Q(z,v)\tilde{s}_r^*(v-\tilde{\tau})\mathrm{d}v\,\mathrm{d}z\right\} - \\ &\left\{\frac{1}{2}\int\limits_{-\infty}^{\infty}\tilde{s}_r(z-\tilde{\tau})\int\limits_{-\infty}^{\infty} Q(z,v)\tilde{s}_r^*(v-\tilde{\tau})\mathrm{d}v\,\mathrm{d}z\right\}.\end{aligned} \tag{A.9}$$

(A.9) can be further simplified by defining

$$g(t,\widetilde{\boldsymbol{\theta}}) \triangleq \int_{-\infty}^{\infty} Q^*(t,v)\tilde{s}_r(v-\tilde{\tau})\mathrm{d}v \tag{A.10}$$

which results in the same expression for log-likelihood function as in (2.10)

$$\ln\Lambda(\widetilde{\boldsymbol{\theta}}) = \Re\left\{\int_{-\infty}^{\infty} r(t)\, g^*(t,\widetilde{\boldsymbol{\theta}})\mathrm{d}t\right\} - \frac{1}{2}\int_{-\infty}^{\infty} \tilde{s}_r(t-\tilde{\tau})\, g^*(t,\widetilde{\boldsymbol{\theta}})\mathrm{d}t. \tag{A.11}$$

The Fourier transform $G(f,\widetilde{\boldsymbol{\theta}})$ of $g(t,\widetilde{\boldsymbol{\theta}})$ can be computed as

$$\begin{aligned}
G(f,\widetilde{\boldsymbol{\theta}}) &= \int_{-\infty}^{\infty} g(t,\widetilde{\boldsymbol{\theta}})e^{-\jmath 2\pi f t}\mathrm{d}t \\
&= \int_{-\infty}^{\infty} \tilde{s}_r(v-\tilde{\tau})\int_{-\infty}^{\infty} Q^*(t,v)e^{-\jmath 2\pi f t}\mathrm{d}t\,\mathrm{d}v \\
&= \int_{-\infty}^{\infty} \tilde{s}_r(v-\tilde{\tau})\int_{-\infty}^{\infty} h^*(u)\int_{-\infty}^{\infty} h(u-v+t)e^{-\jmath 2\pi f t}\mathrm{d}t\,\mathrm{d}u\,\mathrm{d}v \\
&= \int_{-\infty}^{\infty} \tilde{s}_r(v-\tilde{\tau})e^{-\jmath 2\pi f v}\int_{-\infty}^{\infty} h^*(u)e^{\jmath 2\pi f u}\int_{-\infty}^{\infty} h(u-v+t)e^{-\jmath 2\pi f(t+u-v)}\mathrm{d}t\,\mathrm{d}u\,\mathrm{d}v \\
&= \int_{-\infty}^{\infty} h(t)e^{-\jmath 2\pi f t}\mathrm{d}t\int_{-\infty}^{\infty} h^*(u)e^{\jmath 2\pi f u}\mathrm{d}u\int_{-\infty}^{\infty} \tilde{s}_r(v-\tilde{\tau})e^{-\jmath 2\pi f v}\mathrm{d}v \\
&= |H(f)|^2\,\tilde{S}_r(f,\widetilde{\boldsymbol{\theta}}) \\
&= \frac{\tilde{S}_r(f,\widetilde{\boldsymbol{\theta}})}{S_z(f)}
\end{aligned} \tag{A.12}$$

where $\tilde{S}_r(f,\widetilde{\boldsymbol{\theta}})$ is the Fourier transform $\mathscr{F}\{\tilde{s}_r(t-\tilde{\tau})\}$ of $\tilde{s}_r(t-\tilde{\tau})$ in (2.8), and the final expression in (A.12) proves (2.9).

A.3 Elements of FIM in (2.13)

Partial derivatives of

$$\tilde{S}_r(f, \widetilde{\boldsymbol{\theta}}) = \int_{-\infty}^{\infty} \tilde{s}_r(t - \tilde{\tau})\, e^{-\jmath 2\pi f t}\, \mathrm{d}t = \sum_{k=1}^{K} \tilde{a}_k\, e^{\jmath \widetilde{\phi}_k} \sqrt{w_k}\, P(f - f_k)\, e^{-\jmath 2\pi f \tilde{\tau}} \;, \quad \text{(A.13)}$$

with respect to $\tilde{\tau}$, $\tilde{a}_n$, and $\widetilde{\phi}_n$ for $n = 1, 2, \ldots, K$ can be written as

$$\frac{\partial \tilde{S}_r(f, \widetilde{\boldsymbol{\theta}})}{\partial \tilde{\tau}} = -\jmath\, 2\pi f \sum_{k=1}^{K} \tilde{a}_k\, e^{\jmath \widetilde{\phi}_k} \sqrt{w_k}\, P(f - f_k)\, e^{-\jmath 2\pi f \tilde{\tau}} \;, \quad \text{(A.14)}$$

$$\frac{\partial \tilde{S}_r(f, \widetilde{\boldsymbol{\theta}})}{\partial \tilde{a}_n} = e^{\jmath \widetilde{\phi}_n} \sqrt{w_n}\, P(f - f_n)\, e^{-\jmath 2\pi f \tilde{\tau}} \;, \quad \text{(A.15)}$$

$$\frac{\partial \tilde{S}_r(f, \widetilde{\boldsymbol{\theta}})}{\partial \widetilde{\phi}_n} = \jmath\, \tilde{a}_n e^{\jmath \widetilde{\phi}_n} \sqrt{w_n}\, P(f - f_n)\, e^{-\jmath 2\pi f \tilde{\tau}} \;. \quad \text{(A.16)}$$

Defining an auxiliary function

$$y_{m,n}(i) \triangleq \int_{-\infty}^{\infty} \frac{f^i P(f - f_n) P^*(f - f_m)}{S_z(f)} \mathrm{d}f \quad \text{(A.17)}$$

for $i = 0, 1, 2$ and $m, n = 1, 2, \ldots, K$, simplifies the expressions for the elements of FIM $\mathbf{J}$ in (2.13).

$\mathrm{J}_{\tau\tau}$ is a scalar being equal to

$$\begin{aligned}
\mathrm{J}_{\tau\tau} &= \Re \left\{ \int_{-\infty}^{\infty} \frac{\partial \tilde{S}_r^*(f, \widetilde{\boldsymbol{\theta}})}{\partial \tilde{\tau}}\, S_z^{-1}(f)\, \frac{\partial \tilde{S}_r(f, \widetilde{\boldsymbol{\theta}})}{\partial \tilde{\tau}} \mathrm{d}f \right\} \\
&= 4\pi^2 \Re \left\{ \sum_{m=1}^{K} \sum_{n=1}^{K} \tilde{\alpha}_m^* \tilde{\alpha}_n \sqrt{w_m w_n} \int_{-\infty}^{\infty} \frac{f^2 P(f - f_n) P^*(f - f_m)}{S_z(f)} \mathrm{d}f \right\} \quad \text{(A.18)} \\
&= 4\pi^2 \Re \left\{ \sum_{m=1}^{K} \sum_{n=1}^{K} \tilde{\alpha}_m^* \tilde{\alpha}_n \sqrt{w_m w_n}\, y_{m,n}(2) \right\}.
\end{aligned}$$

$\mathbf{J}_{\tau a} = [\mathrm{J}_{\tau \mathrm{a}_1} \cdots \mathrm{J}_{\tau \mathrm{a}_\mathrm{K}}]$ is a $K \times 1$ row vector with entries

$$\begin{aligned}
[\mathbf{J}_{\tau a}]_m &= \Re\left\{ \int_{-\infty}^{\infty} \frac{\partial \tilde{S}_r^*(f, \widetilde{\boldsymbol{\theta}})}{\partial \tilde{\tau}} \, S_z^{-1}(f) \, \frac{\partial \tilde{S}_r(f, \widetilde{\boldsymbol{\theta}})}{\partial \tilde{a}_m} \mathrm{d}f \right\} \\
&= -2\pi\sqrt{w_m}\, \Im\left\{ e^{\jmath \widetilde{\phi}_m} \sum_{k=1}^{K} \tilde{\alpha}_k^* \sqrt{w_k} \int_{-\infty}^{\infty} \frac{f P(f-f_m) P^*(f-f_k)}{S_z(f)} \mathrm{d}f \right\} \qquad \text{(A.19)} \\
&= -2\pi\sqrt{w_m}\, \Im\left\{ e^{\jmath \widetilde{\phi}_m} \sum_{k=1}^{K} \tilde{\alpha}_k^* \sqrt{w_k}\, y_{k,m}(1) \right\}.
\end{aligned}$$

$\mathbf{J}_{\tau \phi} = [\mathrm{J}_{\tau \phi_1} \cdots \mathrm{J}_{\tau \phi_\mathrm{K}}]$ is a $K \times 1$ row vector with entries

$$\begin{aligned}
[\mathbf{J}_{\tau \phi}]_m &= \Re\left\{ \int_{-\infty}^{\infty} \frac{\partial \tilde{S}_r^*(f, \widetilde{\boldsymbol{\theta}})}{\partial \tilde{\tau}} \, S_z^{-1}(f) \, \frac{\partial \tilde{S}_r(f, \widetilde{\boldsymbol{\theta}})}{\partial \widetilde{\phi}_m} \mathrm{d}f \right\} \\
&= -2\pi\sqrt{w_m}\, \Re\left\{ \tilde{\alpha}_m \sum_{k=1}^{K} \tilde{\alpha}_k^* \sqrt{w_k} \int_{-\infty}^{\infty} \frac{f P(f-f_m) P^*(f-f_k)}{S_z(f)} \mathrm{d}f \right\} \qquad \text{(A.20)} \\
&= -2\pi\sqrt{w_m}\, \Re\left\{ \tilde{\alpha}_m \sum_{k=1}^{K} \tilde{\alpha}_k^* \sqrt{w_k}\, y_{k,m}(1) \right\}.
\end{aligned}$$

$\mathbf{J}_{aa}$ is a $K \times K$ matrix

$$\mathbf{J}_{aa} = \begin{bmatrix} \mathrm{J}_{\mathrm{a}_1\mathrm{a}_1} & \mathrm{J}_{\mathrm{a}_1\mathrm{a}_2} & \cdots & \mathrm{J}_{\mathrm{a}_1\mathrm{a}_\mathrm{K}} \\ \mathrm{J}_{\mathrm{a}_2\mathrm{a}_1} & \mathrm{J}_{\mathrm{a}_2\mathrm{a}_2} & \cdots & \mathrm{J}_{\mathrm{a}_2\mathrm{a}_\mathrm{K}} \\ \vdots & \vdots & \ddots & \vdots \\ \mathrm{J}_{\mathrm{a}_\mathrm{K}\mathrm{a}_1} & \mathrm{J}_{\mathrm{a}_\mathrm{K}\mathrm{a}_2} & \cdots & \mathrm{J}_{\mathrm{a}_\mathrm{K}\mathrm{a}_\mathrm{K}} \end{bmatrix}$$

with entries

$$\begin{aligned}
[\mathbf{J}_{aa}]_{m,n} &= \Re\left\{ \int_{-\infty}^{\infty} \frac{\partial \tilde{S}_r^*(f, \widetilde{\boldsymbol{\theta}})}{\partial \tilde{a}_m} \, S_z^{-1}(f) \, \frac{\partial \tilde{S}_r(f, \widetilde{\boldsymbol{\theta}})}{\partial \tilde{a}_n} \mathrm{d}f \right\} \\
&= \sqrt{w_m w_n}\, \Re\left\{ e^{\jmath(\widetilde{\phi}_n - \widetilde{\phi}_m)} \int_{-\infty}^{\infty} \frac{P(f-f_n) P^*(f-f_m)}{S_z(f)} \mathrm{d}f \right\} \qquad \text{(A.21)} \\
&= \sqrt{w_m w_n}\, \Re\left\{ e^{\jmath(\widetilde{\phi}_n - \widetilde{\phi}_m)} y_{m,n}(0) \right\}.
\end{aligned}$$

$\mathbf{J}_{a\phi}$ is a $K \times K$ matrix

$$\mathbf{J}_{a\phi} = \begin{bmatrix} \mathrm{J}_{\mathrm{a}_1\phi_1} & \mathrm{J}_{\mathrm{a}_1\phi_2} & \cdots & \mathrm{J}_{\mathrm{a}_1\phi_\mathrm{K}} \\ \mathrm{J}_{\mathrm{a}_2\phi_1} & \mathrm{J}_{\mathrm{a}_2\phi_2} & \cdots & \mathrm{J}_{\mathrm{a}_2\phi_\mathrm{K}} \\ \vdots & \vdots & \ddots & \vdots \\ \mathrm{J}_{\mathrm{a}_\mathrm{K}\phi_1} & \mathrm{J}_{\mathrm{a}_\mathrm{K}\phi_2} & \cdots & \mathrm{J}_{\mathrm{a}_\mathrm{K}\phi_\mathrm{K}} \end{bmatrix}$$

with entries

$$\begin{aligned} [\mathbf{J}_{a\phi}]_{m,n} &= \Re\left\{ \int_{-\infty}^{\infty} \frac{\partial \tilde{S}_r^*(f,\widetilde{\boldsymbol{\theta}})}{\partial \tilde{a}_m} \, S_z^{-1}(f) \, \frac{\partial \tilde{S}_r(f,\widetilde{\boldsymbol{\theta}})}{\partial \tilde{\phi}_n} \mathrm{d}f \right\} \\ &= -\sqrt{w_m w_n} \, \Im\left\{ e^{-\jmath\tilde{\phi}_m} \tilde{\alpha}_n \int_{-\infty}^{\infty} \frac{P(f-f_n)P^*(f-f_m)}{S_z(f)} \mathrm{d}f \right\} \\ &= -\sqrt{w_m w_n} \, \Im\left\{ e^{-\jmath\tilde{\phi}_m} \tilde{\alpha}_n \, y_{m,n}(0) \right\}. \end{aligned} \tag{A.22}$$

$\mathbf{J}_{\phi\phi}$ is a $K \times K$ matrix

$$\mathbf{J}_{\phi\phi} = \begin{bmatrix} \mathrm{J}_{\phi_1\phi_1} & \mathrm{J}_{\phi_1\phi_2} & \cdots & \mathrm{J}_{\phi_1\phi_\mathrm{K}} \\ \mathrm{J}_{\phi_2\phi_1} & \mathrm{J}_{\phi_2\phi_2} & \cdots & \mathrm{J}_{\phi_2\phi_\mathrm{K}} \\ \vdots & \vdots & \ddots & \vdots \\ \mathrm{J}_{\phi_\mathrm{K}\phi_1} & \mathrm{J}_{\phi_\mathrm{K}\phi_2} & \cdots & \mathrm{J}_{\phi_\mathrm{K}\phi_\mathrm{K}} \end{bmatrix}$$

with entries

$$\begin{aligned} [\mathbf{J}_{\phi\phi}]_{m,n} &= \Re\left\{ \int_{-\infty}^{\infty} \frac{\partial \tilde{S}_r^*(f,\widetilde{\boldsymbol{\theta}})}{\partial \tilde{\phi}_m} \, S_z^{-1}(f) \, \frac{\partial \tilde{S}_r(f,\widetilde{\boldsymbol{\theta}})}{\partial \tilde{\phi}_n} \mathrm{d}f \right\} \\ &= \sqrt{w_m w_n} \, \Re\left\{ \tilde{\alpha}_m^* \tilde{\alpha}_n \int_{-\infty}^{\infty} \frac{P(f-f_n)P^*(f-f_m)}{S_z(f)} \mathrm{d}f \right\} \\ &= \sqrt{w_m w_n} \, \Re\left\{ \tilde{\alpha}_m^* \tilde{\alpha}_n \, y_{m,n}(0) \right\}. \end{aligned} \tag{A.23}$$

A.4 CRB in (2.25)

Under disjoint spectra assumption, $y_{m,n}(i)$ in (A.17) becomes equal to

$$y_{m,n}(i) = \int_{-\infty}^{\infty} \frac{f^i P(f-f_n)P^*(f-f_m)}{S_z(f)} \mathrm{d}f = \begin{cases} \eta_m(i) & , \ \text{if} \quad m = n \\ 0 & , \ \text{if} \quad m \neq n \end{cases} \tag{A.24}$$

where $\eta_m(i)$ is as defined in (2.24)

$$\eta_m(i) = \int_{-\infty}^{\infty} \frac{f^i \left|P(f-f_m)\right|^2}{S_z(f)} \mathrm{d}f \ , \quad i = 0,1,2 \ . \tag{A.25}$$

Hence, the elements of FIM in (A.18)–(A.23) can be expressed as

$$\begin{aligned} \mathrm{J}_{\tau\tau} &= 4\pi^2 \Re \left\{ \sum_{m=1}^{K} \sum_{n=1}^{K} \alpha_m^* \alpha_n \sqrt{w_m w_n}\, y_{m,n}(2) \right\} \\ &= 4\pi^2 \sum_{m=1}^{K} \left|\alpha_m\right|^2 \, w_m \, \eta_m(2) \ , \end{aligned} \tag{A.26}$$

$$\begin{aligned} \left[\mathbf{J}_{\tau a}\right]_m &= -2\pi \sqrt{w_m}\, \Im \left\{ e^{\jmath\phi_m} \sum_{k=1}^{K} \alpha_k^* \sqrt{w_k}\, y_{k,m}(1) \right\} \\ &= -2\pi \sqrt{w_m}\, \Im \left\{ e^{\jmath\phi_m} \, a_m \, e^{-\jmath\phi_m} \sqrt{w_m}\, \eta_m(1) \right\} \\ &= 0 \ , \end{aligned} \tag{A.27}$$

$$\begin{aligned} \left[\mathbf{J}_{\tau\phi}\right]_m &= -2\pi \sqrt{w_m}\, \Re \left\{ \alpha_m \sum_{k=1}^{K} \alpha_k^* \sqrt{w_k}\, y_{k,m}(1) \right\} \\ &= -2\pi \sqrt{w_m}\, \Re \left\{ \alpha_m \alpha_m^* \sqrt{w_m}\, \eta_m(1) \right\} \\ &= -2\pi \, w_m \left|\alpha_m\right|^2 \eta_m(1) \ , \end{aligned} \tag{A.28}$$

$$\begin{aligned} \left[\mathbf{J}_{aa}\right]_{m,n} &= \sqrt{w_m w_n}\, \Re \left\{ e^{\jmath(\phi_n - \phi_m)} y_{m,n}(0) \right\} \\ &= \begin{cases} w_m \, \eta_m(0) & , \ \text{if} \quad m = n \\ 0 & , \ \text{if} \quad m \neq n \end{cases} \ , \end{aligned} \tag{A.29}$$

$$\begin{aligned} \left[\mathbf{J}_{a\phi}\right]_{m,n} &= -\sqrt{w_m w_n}\, \Im \left\{ e^{-\jmath\phi_m} \alpha_n \, y_{m,n}(0) \right\} \\ &= \begin{cases} -w_m \, \Im \left\{ e^{-\jmath\phi_m} a_m e^{\jmath\phi_m} \eta_m(0) \right\} & , \ \text{if} \quad m = n \\ 0 & , \ \text{if} \quad m \neq n \end{cases} \\ &= 0 \ , \end{aligned} \tag{A.30}$$

$$\begin{aligned} \left[\mathbf{J}_{\phi\phi}\right]_{m,n} &= \sqrt{w_m w_n}\, \Re \left\{ \alpha_m^* \alpha_n \, y_{m,n}(0) \right\} \\ &= \begin{cases} w_m \left|\alpha_m\right|^2 \eta_m(0) & , \ \text{if} \quad m = n \\ 0 & , \ \text{if} \quad m \neq n \end{cases} \ . \end{aligned} \tag{A.31}$$

Substitution of (A.27)–(A.31) into the matrices **B** in (2.15) and **C** in (2.16) yields

$$
\begin{aligned}
\mathbf{B} &= \left[\begin{array}{c|c} \mathbf{J}_{\tau a} & \mathbf{J}_{\tau\phi} \end{array}\right] \\
&= \left[\begin{array}{c|c} \mathbf{0} & \mathbf{J}_{\tau\phi} \end{array}\right] \\
&= \left[\begin{array}{ccc|ccc} 0 & \cdots & 0 & -2\pi\, w_1\, |\alpha_1|^2\, \eta_1(1) & \cdots & -2\pi\, w_K\, |\alpha_K|^2\, \eta_K(1) \end{array}\right],
\end{aligned} \tag{A.32}
$$

$$
\begin{aligned}
\mathbf{C} &= \left[\begin{array}{c|c} \mathbf{J}_{aa} & \mathbf{J}_{a\phi} \\ \hline \mathbf{J}_{a\phi}^T & \mathbf{J}_{\phi\phi} \end{array}\right] \\
&= \left[\begin{array}{c|c} \mathbf{J}_{aa} & \mathbf{0} \\ \hline \mathbf{0} & \mathbf{J}_{\phi\phi} \end{array}\right] \\
&= \left[\begin{array}{ccc|ccc}
w_1\,\eta_1(0) & \cdots & 0 & 0 & \cdots & 0 \\
\vdots & \ddots & \vdots & \vdots & \ddots & \vdots \\
0 & \cdots & w_K\,\eta_K(0) & 0 & \cdots & 0 \\
\hline
0 & \cdots & 0 & w_1\,|\alpha_1|^2\,\eta_1(0) & \cdots & 0 \\
\vdots & \ddots & \vdots & \vdots & \ddots & \vdots \\
0 & \cdots & 0 & 0 & \cdots & w_K\,|\alpha_K|^2\,\eta_K(0)
\end{array}\right].
\end{aligned} \tag{A.33}
$$

Then CRB in (2.17) can be computed as

$$
\begin{aligned}
\mathrm{CRB} &= \left(\mathrm{J}_{\tau\tau} - \mathbf{B}\mathbf{C}^{-1}\mathbf{B}^{\mathrm{T}}\right)^{-1} \\
&= \left(\mathrm{J}_{\tau\tau} - \left[\begin{array}{c|c} \mathbf{J}_{\tau a} & \mathbf{J}_{\tau\phi} \end{array}\right] \left[\begin{array}{c|c} \mathbf{J}_{aa} & \mathbf{J}_{a\phi} \\ \hline \mathbf{J}_{a\phi}^T & \mathbf{J}_{\phi\phi} \end{array}\right]^{-1} \left[\begin{array}{c} \mathbf{J}_{\tau a}^T \\ \hline \mathbf{J}_{\tau\phi}^T \end{array}\right]\right)^{-1} \\
&= \left(\mathrm{J}_{\tau\tau} - \left[\begin{array}{c|c} \mathbf{0} & \mathbf{J}_{\tau\phi} \end{array}\right] \left[\begin{array}{c|c} \mathbf{J}_{aa} & \mathbf{0} \\ \hline \mathbf{0}^T & \mathbf{J}_{\phi\phi} \end{array}\right]^{-1} \left[\begin{array}{c} \mathbf{0}^T \\ \hline \mathbf{J}_{\tau\phi}^T \end{array}\right]\right)^{-1} \\
&= \left(\mathrm{J}_{\tau\tau} - \mathbf{J}_{\tau\phi}\mathbf{J}_{\phi\phi}^{-1}\mathbf{J}_{\tau\phi}^{\mathrm{T}}\right)^{-1} \\
&= \left(4\pi^2 \sum_{k=1}^{K} w_k\, |\alpha_k|^2 \left(\eta_k(2) - \frac{\eta_k^2(1)}{\eta_k(0)}\right)\right)^{-1} \\
&= \left(\sum_{k=1}^{K} w_k\, \lambda_k,\right)^{-1}
\end{aligned} \tag{A.34}
$$

where λ_k is as defined in (2.26).

A.5 λ_k in (2.30)

Under the assumptions of disjoint spectra, and slowly varying total disturbance power spectral density $S_z(f)$, $\eta_k(i)$ in (2.24) becomes

$$\begin{aligned}\eta_k(i) &\cong \frac{1}{S_z(f_k)} \int_{-\infty}^{\infty} f^i \left|P(f-f_k)\right|^2 \mathrm{d}f \\ &= \frac{1}{S_z(f_k)} \int_{f_k-\Delta/2}^{f_k+\Delta/2} f^i \left|P(f-f_k)\right|^2 \mathrm{d}f \\ &= \frac{1}{S_z(f_k)} \int_{-\Delta/2}^{\Delta/2} (f+f_k)^i \left|P(f)\right|^2 \mathrm{d}f, \quad i=0,1,2.\end{aligned} \tag{A.35}$$

Then $\eta_k(i)$ for $i = 0, 1, 2$ can be expressed as

$$\begin{aligned}\eta_k(2) &= \frac{E_p}{S_z(f_k)} \left(\frac{1}{E_p} \int_{-\Delta/2}^{\Delta/2} f^2 \left|P(f)\right|^2 \mathrm{d}f + \frac{2f_k}{E_p} \int_{-\Delta/2}^{\Delta/2} f \left|P(f)\right|^2 \mathrm{d}f + \frac{f_k^2}{E_p} \int_{-\Delta/2}^{\Delta/2} \left|P(f)\right|^2 \mathrm{d}f \right) \\ &= \frac{E_p}{S_z(f_k)} \left(\beta_2 + 2f_k\beta_1 + f_k^2\right) \ ,\end{aligned} \tag{A.36}$$

$$\begin{aligned}\eta_k(1) &= \frac{E_p}{S_z(f_k)} \left(\frac{1}{E_p} \int_{-\Delta/2}^{\Delta/2} f \left|P(f)\right|^2 \mathrm{d}f + \frac{f_k}{E_p} \int_{-\Delta/2}^{\Delta/2} \left|P(f)\right|^2 \mathrm{d}f \right) \\ &= \frac{E_p}{S_z(f_k)} \left(\beta_1 + f_k\right) \ ,\end{aligned} \tag{A.37}$$

$$\begin{aligned}\eta_k(0) &= \frac{E_p}{S_z(f_k)} \left(\frac{1}{E_p} \int_{-\Delta/2}^{\Delta/2} \left|P(f)\right|^2 \mathrm{d}f \right) \\ &= \frac{E_p}{S_z(f_k)} \ ,\end{aligned} \tag{A.38}$$

where β_i is as defined in (2.28).

Substitution of (A.36)-(A.38) into λ_k in (2.26) gives (2.30) which is

$$\begin{aligned} \lambda_k &= 4\pi^2 \left|\alpha_k\right|^2 \left(\eta_k(2) - \frac{\eta_k^2(1)}{\eta_k(0)}\right) \\ &= \frac{4\pi^2 E_p \left|\alpha_k\right|^2 \left(\beta_2 - \beta_1^2\right)}{N_0 + S_I(f_k)} \; . \end{aligned} \tag{A.39}$$

A.6 Proof of Proposition 1

We show that (2.40) is the solution of the maximization problem (2.35) subject to the constraints (2.36)–(2.38). The proof is recursive [39], i.e., we first show that $w_1^{(\mathrm{opt})} = \min\{1, b_1\}$, then $w_2^{(\mathrm{opt})} = \min\left\{1 - w_1^{(\mathrm{opt})}, b_2\right\}$, next $w_3^{(\mathrm{opt})} = \min\left\{1 - w_1^{(\mathrm{opt})} - w_2^{(\mathrm{opt})}, b_3\right\}$, and so on.

We begin with proving that $w_1^{(\mathrm{opt})} = \min\{1, b_1\}$. As a first step in this direction we observe that $w_1^{(\mathrm{opt})}$ must be smaller than or equal to $\min\{1, b_1\}$. This is so because (2.36)–(2.37) require $w_1^{(\mathrm{opt})} \leq 1$, while (2.38) requires $w_1^{(\mathrm{opt})} \leq b_1$. Thus, it must be

$$w_1^{(\mathrm{opt})} = \min\{1, b_1\} - \delta \; , \qquad \delta \geq 0 \; . \tag{A.40}$$

We maintain that assuming $\delta > 0$ leads to a contradiction. In fact, we show that, if the optimal solution $\boldsymbol{w}^{(\mathrm{opt})} = \left(w_1^{(\mathrm{opt})}, w_2^{(\mathrm{opt})}, \ldots, w_K^{(\mathrm{opt})}\right)^T$ has the first component smaller than $\min\{1, b_1\}$, then a vector $\boldsymbol{w}$ can be found that satisfies (2.36)–(2.38) and has a scalar product $\boldsymbol{\lambda}^T \boldsymbol{w}$ greater than $\boldsymbol{\lambda}^T \boldsymbol{w}^{(\mathrm{opt})}$.

To proceed, we distinguish two cases, say (a) and (b), according to whether δ is smaller or greater than $\sum_{k=2}^{n} w_k^{(\mathrm{opt})}$.

A.6.1 Case $(\boldsymbol{a})$

Assume

$$0 < \delta \leq \sum_{k=2}^{n} w_k^{(\mathrm{opt})} \tag{A.41}$$

and introduce the parameter

$$\alpha \triangleq \frac{\delta}{\sum\limits_{k=2}^{n} w_k^{(\mathrm{opt})}} . \tag{A.42}$$

Note that $0 < \alpha \leq 1$. Now consider a vector $\boldsymbol{w}$ such that

$$w_1 = \min\{1, b_1\} \tag{A.43}$$

and

$$w_k = (1-\alpha) w_k^{(\mathrm{opt})} , \qquad k = 2, 3, \ldots, K . \tag{A.44}$$

Such a vector satisfies (2.37) because its components are all non-negative. It also satisfies (2.38) because $w_1 \leq b_1$ (see (A.43)) and $w_k < w_k^{(\mathrm{opt})} \leq b_k$ ($k = 2, 3, \ldots, K$) as consequence of (A.44). Finally, it satisfies (2.36) because from (A.43)–(A.44) it is found that $\mathbf{1}^T \boldsymbol{w} = \mathbf{1}^T \boldsymbol{w}^{(\mathrm{opt})} \leq 1$.

Next consider the scalar product $\boldsymbol{\lambda}^T \boldsymbol{w}$. We have

$$\begin{aligned}
\boldsymbol{\lambda}^T \boldsymbol{w} &= \lambda_1 \min\{1, b_1\} + \sum_{k=2}^{K} \lambda_k w_k \\
&= \lambda_1 \min\{1, b_1\} + \sum_{k=2}^{K} \lambda_k (1-\alpha) w_k^{(\mathrm{opt})} \\
&= \lambda_1 \min\{1, b_1\} + \sum_{k=2}^{K} \lambda_k w_k^{(\mathrm{opt})} - \alpha \sum_{k=2}^{K} \lambda_k w_k^{(\mathrm{opt})} \\
&> \lambda_1 \min\{1, b_1\} + \sum_{k=2}^{K} \lambda_k w_k^{(\mathrm{opt})} - \alpha \lambda_1 \sum_{k=2}^{K} w_k^{(\mathrm{opt})} \\
&= \lambda_1 \min\{1, b_1\} + \sum_{k=2}^{K} \lambda_k w_k^{(\mathrm{opt})} - \lambda_1 \delta \\
&= \boldsymbol{\lambda}^T \boldsymbol{w}^{(\mathrm{opt})}
\end{aligned} \tag{A.45}$$

where the passage from the third to the fourth line follows from the fact that λ_1 is the largest λ_k, while the passage from the fourth to the fifth line is a consequence of (A.42). Equation (A.45) indicates a contradiction since $\boldsymbol{\lambda}^T \boldsymbol{w}^{(\mathrm{opt})}$ is the maximum possible value of $\boldsymbol{\lambda}^T \boldsymbol{w}$.

A.6.2 Case (b)

Suppose

$$\delta > \sum_{k=2}^{n} w_k^{(\mathrm{opt})} \tag{A.46}$$

and consider a vector $\boldsymbol{w}$ such that w_1 is as in (A.43) while

$$w_k \triangleq 0 \ , \qquad k = 2, 3, \ldots, K \ . \tag{A.47}$$

As in the previous case, it is easily checked that $\boldsymbol{w}$ satisfies conditions (2.36)–(2.38). On the other hand, we have

$$\boldsymbol{\lambda}^T \boldsymbol{w} = \lambda_1 \min\{1, b_1\} \ , \tag{A.48}$$

while

$$\begin{aligned} \boldsymbol{\lambda}^T \boldsymbol{w}^{(\mathrm{opt})} &= \lambda_1 \left(\min\{1, b_1\} - \delta\right) + \sum_{k=2}^{K} \lambda_k w_k^{(\mathrm{opt})} \\ &= \lambda_1 \min\{1, b_1\} - \lambda_1 \delta + \sum_{k=2}^{K} \lambda_k w_k^{(\mathrm{opt})} \\ &< \lambda_1 \min\{1, b_1\} - \lambda_1 \delta + \lambda_1 \sum_{k=2}^{K} w_k^{(\mathrm{opt})} \\ &= \lambda_1 \min\{1, b_1\} - \lambda_1 \left(\delta - \sum_{k=2}^{K} w_k^{(\mathrm{opt})}\right) \\ &< \lambda_1 \min\{1, b_1\} \\ &= \boldsymbol{\lambda}^T \boldsymbol{w} \end{aligned} \tag{A.49}$$

where the passage from the second to the third line follows from the fact that λ_1 is the largest λ_k, while the passage from the fourth to the fifth and the sixth lines is a consequence of (A.46) and (A.48). Again we see that $\boldsymbol{\lambda}^T \boldsymbol{w} > \boldsymbol{\lambda}^T \boldsymbol{w}^{(\mathrm{opt})}$, which is a contradiction. Putting the cases (a) and (b) together, we conclude that it must be $w_1^{(\mathrm{opt})} = \min\{1, b_1\}$.

Next we look for the remaining components of $\boldsymbol{w}^{(\mathrm{opt})}$. Defining the $(K-1)$-dimensional vectors $\boldsymbol{\lambda}' \triangleq [\lambda_2 \cdots \lambda_K]^T$, $\boldsymbol{b}' \triangleq [b_2 \cdots b_K]^T$,and $\boldsymbol{w}' \triangleq$

$[w_2 \cdots w_K]^T$, our task is to solve the following optimization problem:

$$\underset{\boldsymbol{w}}{\text{maximize}} \quad \boldsymbol{\lambda}'^T \boldsymbol{w}' \tag{A.50}$$

subject to

$$\mathbf{1}^T \boldsymbol{w}' \leq 1 - w_1^{(\text{opt})} \tag{A.51}$$

$$\boldsymbol{w}' \succeq \mathbf{0} \tag{A.52}$$

$$\boldsymbol{w}' \preceq \boldsymbol{b}' \tag{A.53}$$

Reasoning as before, the first component of the optimal solution is found to be $\min\left\{1 - w_1^{(\text{opt})}, b_2\right\}$. Thus, we have $w_2^{(\text{opt})} = \min\left\{1 - w_1^{(\text{opt})}, b_2\right\}$. Proceeding in this way, with the other components of $\boldsymbol{w}^{(\text{opt})}$, produces the full solution in (2.39). $\square$

Bibliography

[1] J. Mitola and G. Q. Maguire, "Cognitive radio: Making software radios more personal," *IEEE Personal Communications*, vol. 6, pp. 13–18, Aug. 1999.

[2] S. Haykin, "Cognitive radio: Brain-empowered wireless communications," *IEEE Journal on Selected Areas in Communications*, vol. 23, no. 2, pp. 201–220, Feb. 2005.

[3] Z. Quan, S. Cui, H. V. Poor, and A. H. Sayed, "Collaborative wideband sensing for cognitive radios," *IEEE Signal Processing Magazine*, vol. 25, no. 6, pp. 60–73, Nov. 2008.

[4] J. O. Neel, *Analysis and design of cognitive radio networks and distributed radio resource management algorithms.* PhD dissertation, Virginia Polytechnic Institute and State University, VA, Sept. 2006.

[5] Q. Zhao and B. M. Sadler, "A survey of dynamic spectrum access," *IEEE Signal Processing Magazine*, vol. 24, no. 3, pp. 79–89, May. 2007.

[6] A. Giorgetti, M. Chiani, D. Dardari, R. Piesiewicz, and G. H. Bruk, "The cognitive radio paradigm for ultra-wideband systems: the European Project EUWB," in *Proceedings of IEEE International Conference on Ultra-Wideband (ICUWB)*, vol. 2, (Hannover, Germany), pp. 169–172, Sept. 2008.

[7] H. Arslan (Ed.), *Cognitive Radio, Software Defined Radio, and Adaptive Wireless Systems.* Springer, Sept. 2007.

[8] Federal Communications Commission (FCC), "Facilitating opportunities for flexible, efficient, and reliable spectrum use employing cognitive radio technologies," Tech. Rep. ET Docket No. 03-108, Mar. 2005.

[9] M. Wellens, J. Wu, and P. Mahonen, "Evaluation of spectrum occupancy in indoor and outdoor scenario in the context of cognitive radio," in *Proceedings of 2nd International Conference on Cognitive Radio Oriented Wireless Networks and Communications (CROWNCOM)*, (Orlando, FL), pp. 420–427, Aug. 2007.

[10] F. Kocak, H. Celebi, S. Gezici, K. A. Qaraqe, H. Arslan, and H. V. Poor, "Time delay estimation in dispersed spectrum cognitive radio systems," *EURASIP Journal on Advances in Signal Processing (Special Issue on Advanced Signal Processing for Cognitive Radio Networks)*, 2010.

[11] H. Celebi and H. Arslan, "Enabling location and environment awareness in cognitive radios," *Elsevier Computer Communications (Special Issue on Advanced Location-Based Services)*, vol. 31, no. 6, pp. 1114–1125, Apr. 2008.

[12] H. Celebi and H. Arslan, "Cognitive positioning systems," *IEEE Transactions on Wireless Communications*, vol. 6, no. 12, pp. 4475–4483, Dec. 2007.

[13] S. Haykin, "Cognitive radar: A way of the future," *IEEE Signal Processing Magazine*, vol. 23, no. 1, pp. 30–40, Jan. 2006.

[14] Y. Zhao, H. H. Reed, S. Mao, and K. K. Bae, "Overhead analysis for radio environment map–enabled cognitive radio networks," in *Proceedings of 1st IEEE Workshop on Networking Technologies for Software Defined Radio Networks*, (Reston, VA), pp. 18–25, Sept. 2006.

[15] S. Yarkan and H. Arslan, "Exploiting location awareness towards improved wireless system design in cognitive radio," *IEEE Communications Magazine*, vol. 46, no. 1, pp. 128–136, Jan. 2008.

[16] P. Mahonen, M. Petrova, , and J. Riihijarvi, "Applications of topology information for cognitive radios and networks," in *Proceedings of 2nd IEEE International Symposium on New Frontiers in Dynamic Spectrum Access Networks (DySpan)*, (Dublin, Ireland), pp. 103–114, Apr. 2007.

[17] H. Celebi and H. Arslan, "Adaptive positioning systems for cognitive radios," in *Proceedings of 2nd IEEE International Symposium on New Frontiers in Dynamic Spectrum Access Networks (DySPAN)*, (Dublin, Ireland), pp. 78–84, Apr. 2007.

[18] H. Celebi and H. Arslan, "Utilization of location information in cognitive wireless networks," *IEEE Wireless Commununications*, vol. 14, no. 4, pp. 6–13, Aug. 2007.

[19] D. Dardari, A. Conti, U. Ferner, A. Giorgetti, and M. Z. Win, "Ranging with ultrawide bandwidth signals in multipath environments," *Proceedings of IEEE Special Issue on UWB Technology and Emerging Applications*, vol. 97, no. 2, pp. 404–426, Feb. 2009.

[20] S. Gezici, "A survey on wireless position estimation," *Wireless Personal Communications, Special Issue on Towards Global and Seamless Personal Navigation*, vol. 44, no. 3, pp. 263–282, Feb. 2008.

[21] Z. Sahinoglu, S. Gezici, and I. Guvenc, *Ultra-Wideband Positioning Systems.* New York: Cambridge University Press, Oct. 2008.

[22] Y. Shen, H. Wymeersch, and M. Z. Win, "Fundamental limits of wideband cooperative localization via Fisher Information," in *Proceedings of IEEE Wireless Communications and Networking Conference (WCNC 2007)*, (Knowloon, China), pp. 3951–3955, Mar. 2007.

[23] S. Gezici, H. Celebi, H. V. Poor, and H. Arslan, "Fundamental limits on time delay estimation in dispersed spectrum cognitive radio systems," *IEEE*

Transactions on Wireless Communications, vol. 8, no. 1, pp. 78–83, Jan. 2009.

[24] T. A. Weiss and F. K. Jondral, "Spectrum pooling: An innovative strategy for the enhancement of spectrum efficiency," *IEEE Communications Magazine*, vol. 42, no. 3, pp. 8–14, Mar. 2004.

[25] S. Brandes, I. Cosovic, and M. Schnell, "Reduction of out-of-band radiation in OFDM based overlay systems," in *Proceedings of First International Symposium on New Frontiers in Dynamic Spectrum Access Networks DySPAN*, (Baltimore, MD), pp. 662–665, Nov. 2005.

[26] H. A. Mahmoud and H. Arslan, "Sidelobe suppression in OFDM-based spectrum sharing systems using adaptive symbol transition," *IEEE Communications Letters*, vol. 12, no. 2, pp. 133–135, Feb. 2008.

[27] D. Dardari, "Ordered subcarrier selection algorithm for OFDM based high-speed WLANs," *IEEE Transactions on Wireless Communications*, vol. 3, no. 5, pp. 1452–1458, Sept. 2004.

[28] D. Dardari, Y. Karisan, S. Gezici, A. A. D'Amico, and U. Mengali, "Performance limits on ranging with cognitive radio," in *Proceedings of IEEE International Conference on Communications (ICC) Workshop*, (Dresden, Germany), pp. 649–653, June 2009.

[29] S. Gault, W. Hachem, and P. Ciblat, "Joint sampling clock offset and channel estimation for OFDM signals: Cramer-rao bound and algorithms," *IEEE Transactions on Signal Processing*, vol. 54, no. 5, pp. 1875–1885, May. 2006.

[30] Z. J. Wang, Z. Han, and K. J. R. Liu, "A MIMO-OFDM channel estimation approach using time of arrivals," *IEEE Transactions on Wireless Communications*, vol. 4, no. 3, pp. 1207–1213, May. 2005.

[31] A. Goldsmith, *Wireless Communications*. Cambridge University Press, Aug. 2005.

[32] B. Z. Bobrovsky, E. Mayer-Wolf, and M. Zakai, “Some classes of global Cramér-Rao bounds,” *The Annals of Statistics*, vol. 15, no. 4, pp. 1421–1438, 1987.

[33] H. L. Van Trees, *Detection, Estimation, and Modulation Theory, Part I.* John Wiley & Sons Inc, June 1963.

[34] S. M. Kay, *Fundamentals of Statistical Signal Processing Volume I: Estimation Theory.* Prentice Hall, Apr. 1993.

[35] J. Zhang, R. A. Kennedy, and T. D. Abhayapala, “Cramer-Rao lower bounds for the synchronization of UWB signals,” *EURASIP Journal on Applied Signal Processing*, vol. 3, pp. 426–438, 2005.

[36] Federal Communications Commission (FCC), “First report and order,” Tech. Rep. 02-48, Feb. 2002.

[37] H. V. Poor, *An Introduction to Signal Detection and Estimation.* New York: Springer-Verlag, 1994.

[38] J. Proakis, *Digital Communications.* 4th Edition, McGraw-Hill, Aug. 2000.

[39] Y. Karisan, D. Dardari, S. Gezici, A. A. D’Amico, and U. Mengali, “Performance limits on range estimation in cognitive radio systems,” submitted, Nov. 2009. [Available: www.ee.bilkent.edu.tr/∼gezici/yasir.pdf].